Complex-scaling method for the plasmonic resonances of planar subwavelength particles with corners

Anne-Sophie Bonnet-Ben Dhia, Christophe Hazard, Florian Monteghetti

Complex-scaling method for the plasmonic resonances of planar subwavelength particles with corners

Anne-Sophie Bonnet-Ben Dhia[a], Christophe Hazard[a], Florian Monteghetti[a,*]

[a] *POEMS (CNRS-INRIA-ENSTA Paris), Institut Polytechnique de Paris, Palaiseau, France*

Abstract

A subwavelength metallic particle supports surface plasmons for some negative permittivity values, which are eigenvalues of the self-adjoint quasi-static plasmonic eigenvalue problem (PEP). This work investigates the existence of complex plasmonic resonances for a 2D particle whose boundary is smooth except for one straight corner. These resonances are defined using the multivalued nature of some zeros of the corner dispersion relations and they are shown to be eigenvalues of a PEP that is complex-scaled at the corner, the finite element discretization of which yields a linear generalized eigenvalue problem. Numerical results show that the complex scaling deforms the essential spectrum (associated with the corner) so as to unveil both embedded plasmonic eigenvalues and complex plasmonic resonances. The later are analogous to complex scattering resonances with the local behavior at the corner playing the role of the behavior at infinity. These results corroborate the study of Li and Shipman (J. Integral Equ. Appl. 31(4), 2019), which proved the existence of embedded plasmonic eigenvalues and discussed the construction of particles that exhibit complex plasmonic resonances.

Keywords: plasmonics, Neumann-Poincaré operator, complex resonances, embedded eigenvalues, complex scaling, perfectly matched layer, *2010 PACS:* 73.20.Mf, *2010 MSC:* 35P99

Preprint August 26, 2020

1. Introduction

The broad focus of this paper is the quasi-static plasmonic eigenvalue problem (PEP) for planar domains with corners. We consider a plasmonic particle Ω_m (typically made of metal), assumed to be a piecewise-smooth open set, surrounded by a dielectric medium $\Omega_d := \mathbb{R}^2 \backslash \overline{\Omega_m}$. If u denotes the electric field potential, then the strong form of the PEP is: find (u, κ) such that

$$\Delta u(\boldsymbol{x}) = 0 \quad (\boldsymbol{x} \in \Omega_m \cup \Omega_d)\,, \tag{1}$$

with the transmission boundary conditions

$$u_{|\Omega_m}(\boldsymbol{x}) = u_{|\Omega_d}(\boldsymbol{x}),\ \partial_n u_{|\Omega_m}(\boldsymbol{x}) = \kappa\, \partial_n u_{|\Omega_d}(\boldsymbol{x}) \quad (\boldsymbol{x} \in \partial\Omega_m)\,, \tag{2}$$

where $\boldsymbol{n}$ denotes a unit normal defined on $\partial\Omega_m$, and the decay condition at infinity

$$u(\boldsymbol{x}) \underset{|\boldsymbol{x}|\to\infty}{=} O\left(|\boldsymbol{x}|^{-1}\right) \tag{3}$$

to exclude the trivial solutions $(u = \mathrm{cst}, \kappa)$ [1, § 2.4].

The spectral parameter κ, known as the *contrast*, is the ratio of dielectric permittivity across the interface $\partial\Omega_m$. Physically κ depends upon the angular frequency ω, the simplest classical model being that of a free electron gas known as Drude's model [2, Eq. (6.18)] [3, Eq. (7.56)]. However this dependency is not considered further herein since ω does not appear explicitly in the quasi-static approximation (1). Solutions of the PEP (1,2,3) are surface

*Corresponding author
Email address: florian.monteghetti@ensta-paris.fr (Florian Monteghetti)

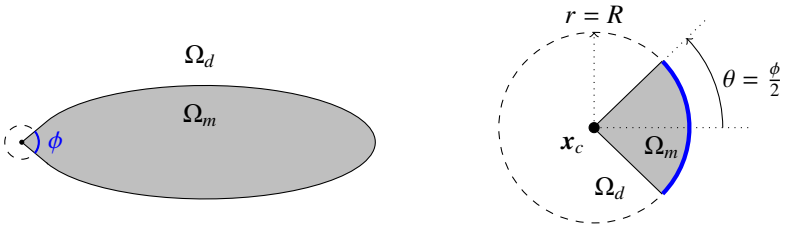

(a) Overview with corner neighborhood highlighted. (b) Corner neighborhood $D := \{|\boldsymbol{x} - \boldsymbol{x}_c| < R\}$.

Fig. 1: Particle Ω_m and dielectric medium Ω_d. The sign-changing interface $\partial\Omega_m$ is smooth except for a straight corner of angle ϕ.

waves known as *surface plasmons*, whose energy-concentrating properties are commonly used today in label-free chemical and biological sensors with applications in areas as diverse as pollution monitoring, medical diagnostic, pharmaceutical development, and toxicology [4] [5, Chap. 11] [6]. Surface plasmons also have high-potential applications in photonics [7, 8], such as subwavelength or "perfect" lenses [9, § 3] [10, § 4].

The presence of corners in $\partial\Omega_m$ implies theoretical and numerical difficulties, which have been studied within different bodies of literature surveyed below.

1.1. Analysis and discretization of the PEP weak formulation

A formal integration by parts of the PEP (1,2,3) yields: find (u, κ) such that, for any test function v,

$$\int_{\Omega_m} \nabla u(\boldsymbol{x}) \cdot \nabla v(\boldsymbol{x}) \, \mathrm{d}\boldsymbol{x} = -\kappa \int_{\Omega_d} \nabla u(\boldsymbol{x}) \cdot \nabla v(\boldsymbol{x}) \, \mathrm{d}\boldsymbol{x},$$

which is a generalized eigenvalue problem. Taking $v = \overline{u}$ shows that $\kappa \leq 0$, i.e. the permittivity changes sign: the interface $\partial\Omega_m$ is said to be *sign-changing*. This complicates the analysis of well-posedness as well as discretization since ellipticity is lost (the weak formulation is coercive if and only if $\kappa \notin (-\infty, 0]$ [11, § 3]). A crucial result is that the topology of the spectrum depends on the interface's smoothness. If $\partial\Omega_m$ is smooth then the spectrum consists of a sequence of distinct eigenvalues κ_n that accumulates at -1 [1, Thm. 1]. The closer κ_n is to -1, the more oscillating and localized (at the surface) the corresponding H^1_{loc} eigenfunction is, as illustrated in Figure 9.

However, if the interface has a corner of angle $\phi \in (0, \pi)$ (as illustrated in Figure 1a), then the spectrum contains in addition the *critical interval* [12, 11]

$$I_c = \left(-\frac{2\pi - \phi}{\phi}, -1\right) \cup \left(-1, -\frac{\phi}{2\pi - \phi}\right) \subset (-\infty, 0),$$

which can be interpreted as essential spectrum [13, Thm. 3] [14]. Each contrast κ in the critical interval is associated with a pair of strongly-oscillating surface waves, conjugate of each other, depicted in Figure 2. A peculiar feature of these two waves is that they do not have finite energy (i.e. they belong to L^2 but not H^1 around the corner). Physical insights can be gained by working in the Euler coordinates (z, θ), deduced from the polar coordinates centered at the corner by $(z = \ln r, \theta)$, which send the corner $r = 0$ to infinity $z = -\infty$: the two waves have opposite group velocities and can be interpreted as radiating energy either "to" or "from" the corner, each respecting a different radiation condition at $z \to -\infty$ [11]. The "outgoing" wave, which is the one needed to satisfy the limiting absorption principle, has been called a *black-hole* wave [11] since it effectively traps energy at the corner.

Numerically, this analysis has been used to design a perfectly matched layer (PML) that selects the desired wave at the corner. This corner PML has been demonstrated on a finite element (FE) discretization of the plasmonic scattering problem with $\kappa \in I_c$ in [15], where it is shown to yield a convergent discretization. In the physics literature, FE discretizations of (1,2) without corner PML have been considered, see e.g. [16].

1.2. Analysis and discretization of the PEP integral formulation (Neumann-Poincaré operator)

By looking for u as a single-layer potential $u = \mathcal{S}[\varphi]$, an integral formulation of the PEP (1,2,3) can be obtained by combining the jump property [17, Thm. 3.28] [18, Chap. 3] with the transmission conditions (2): find (φ, λ) such that [19, Eq. (4)] [20, Thm. 2.1]

$$\mathcal{K}^\star \varphi = \lambda \varphi, \tag{4}$$

where the operator $\mathcal{K}^\star$ is the adjoint of the double-layer potential, also known as the Neumann-Poincaré (NP) operator, and the link between the spectral parameter λ and the contrast κ is given by

$$\lambda = \frac{1}{2} \times \frac{1+\kappa}{1-\kappa}, \ \kappa = \frac{2\lambda - 1}{2\lambda + 1}.$$

The integral formulation of the non quasi-static case is derived in [21, Eq. (2.3)].

Numerically, boundary element (BE) methods have been used in the physics literature to solve the PEP, see [22] for instance. A detailed comparative study of BE methods for particles with corners is available in [23]. Theoretically, the NP operator has enjoyed a renewed scrutiny stimulated by the interest in plasmonics: see e.g. [24] for an optimal shape design problem, [25] for a mathematical study of surface plasmons, [26] for an investigation into the validity of the quasi-static approximation, [27] for a study of the rate of resonance, and [28] for a spectral resolution of the NP operator on intersecting disks.

Let us now review some results of spectral theory: in agreement with Section 1.1, the spectrum of the NP operator depends upon the smoothness of the interface. For a Lipschitz boundary, $\mathcal{K}^\star$ is a bounded self-adjoint operator.[1] If the interface is smooth then $\mathcal{K}^\star$ is compact and its spectrum consists of a sequence of eigenvalues λ_n that accumulates at $\lambda = 0$ ($\kappa = -1$). If the interface has a corner of angle $\phi \in (0, \pi)$ then $\mathcal{K}^\star$ loses its compactness: its essential spectrum is given by [31, Thm. 7] (see also [32, Eq. (7)])

$$\sigma_{\text{ess}}\left(\mathcal{K}^\star\right) = \left[\frac{\phi-\pi}{2\pi}, \frac{\pi-\phi}{2\pi}\right] = \left\{\lambda = \frac{1}{2} \times \frac{1+\kappa}{1-\kappa} \,\middle|\, \kappa \in \overline{I_c}\right\} \subset \left(-\frac{1}{2}, \frac{1}{2}\right)$$

and its eigenvalues λ_n can only accumulate at 0 and $\pm\frac{\phi-\pi}{2\pi}$ [33, Thm. A].

A numerical investigation into the different components of $\sigma(\mathcal{K}^\star)$ using a rate-of-resonance criterion showed the presence of embedded eigenvalues for an elliptical particle perturbed by a corner [34]. It is proven in [35, Thm. 8] that given a symmetric closed $\mathcal{C}^2$ interface, there exists a corner perturbation that generates embedded eigenvalues. Moreover, in [35, § 5.2] it is suggested that this corner perturbation can lead to some eigenvalues crossing the essential spectrum to become complex resonances: this will be confirmed using complex scaling in Section 5.

1.3. Outline

The objective of this paper is to investigate the existence of so-called *complex plasmonic resonances* for a 2D subwavelength particle whose boundary is smooth except for one straight corner. We first propose a definition of complex plasmonic resonances that relies solely on an analysis of the corner dispersion relations. We then show that complex plasmonic resonances are eigenvalues of the PEP (1,2,3) subjected to a corner complex scaling. A FE discretization of this complex-scaled PEP yields a complex-symmetric linear generalized eigenvalue problem.

In the footsteps of [34, 35], the numerical application focuses on an elliptical particle perturbed by a corner. Results show that the complex scaling deforms the critical interval I_c so as to unveil both embedded plasmonic eigenvalues and complex plasmonic resonances. The latter are associated with surface plasmons (named herein *complex plasmonic resonance functions*) whose behavior at the corner $\boldsymbol{x}_c$ is

$$u(\boldsymbol{x}) \underset{|\boldsymbol{x}-\boldsymbol{x}_c|\to 0}{\sim} \frac{1}{|\boldsymbol{x}-\boldsymbol{x}_c|^{\mathfrak{I}(\eta)}} \quad (\mathfrak{I}(\eta) > 0)\,.$$

Complex plasmonic resonances are formally analogous to complex scattering resonances, with the local behavior at the corner playing the role of the behavior at infinity. These results corroborate the study [35], which proved the existence of embedded plasmonic eigenvalues and discussed the construction of particles that exhibit complex plasmonic resonances.

This paper is organized as follows. Section 2 defines complex plasmonic resonances. To compute them, we rely on a corner complex scaling that is recalled and analyzed in Section 3. Section 4 validates the proposed FE formulation and emphasizes the discretization challenges inherent to the sign-changing nature of the interface. Lastly, Section 5 gathers the numerical results. The proofs of some technical or known results are gathered in Appendices A, B, and D. Appendix C contains further comments on the definition of complex plasmonic resonances proposed herein.

[1] When considered as an operator from $H^{-1/2}(\partial\Omega_m)$ to itself, equipped with the inner product induced by the single-layer potential $\mathcal{S}$: this technical result is a consequence of Plemelj's symmetrization principle [29] [30, Thm. 2.5].

Remark 1 (On the meaning of "complex resonance"). In this paper, the denomination "complex resonance" is used in the sense of [36, 37]. The complex resonances defined and computed in this work are designated "complex plasmonic resonances" to distinguish them from "complex scattering resonances". This terminology will be defined in Section 2.2.3, but to avoid confusion let us emphasize now that "complex resonance" and "complex resonance function" are different concepts from "complex eigenvalue" and "eigenfunction". In the physical literature, "complex resonance functions" are sometimes also called "quasi-normal modes".

2. Basics of corner plasmonics and definition of complex plasmonic resonances

The purpose of this section is to define complex plasmonic resonances. Section 2.1 recalls the "trinity of corner plasmonics": the corner dispersion relations (7), the associated sets of zeros (8), and the critical interval (10). Section 2.2 then defines complex plasmonic resonances in Definition 13. The proposed definition is computational inasmuch as it relies explicitly on the asymptotic expansion at the corner, which will ease the introduction of the complex-scaling technique in Section 3.

Assumption. Throughout Sections 2 and 3 the particle Ω_m is an open set with a boundary $\partial\Omega_m$ that is smooth except at $\boldsymbol{x}_c$, where there is a straight corner of angle $\phi \in (0, 2\pi)\backslash\{\pi\}$, see Figure 1a for an example.

Notation. The dielectric medium is $\Omega_d := \mathbb{R}^2\backslash\overline{\Omega_m}$. Let

$$\kappa_\phi := -\frac{2\pi-\phi}{\phi},\ D := \{|\boldsymbol{x}-\boldsymbol{x}_c| < R\},\ \Theta_m := \left(-\frac{\phi}{2}, \frac{\phi}{2}\right),\ \Theta_d := \left(-\pi, -\frac{\phi}{2}\right) \cup \left(\frac{\phi}{2}, \pi\right]. \tag{5}$$

The radius $R > 0$ is small enough so that D only includes the straight corner. The polar coordinates (r, θ) with $\theta \in (-\pi, \pi]$ are centered at $\boldsymbol{x}_c$, see the sketch of Figure 1b. The set $D_m := \Omega_m \cap D$ (resp. $D_d := \Omega_d \cap D$) is described by $r < R$ and $\theta \in \Theta_m$ (resp. $\theta \in \Theta_d$).

2.1. Corner dispersion relations and critical interval

To define complex plasmonic resonances we first "zoom at the corner", i.e. we carry out a local study near the corner by considering

$$\begin{cases} \Delta u(\boldsymbol{x}) = 0 \quad (\boldsymbol{x} \in D_m \cup D_d) \\ u_{|D_m}(\boldsymbol{x}) = u_{|D_d}(\boldsymbol{x}),\ \partial_n u_{|D_m}(\boldsymbol{x}) = \kappa\, \partial_n u_{|D_d}(\boldsymbol{x}) \quad (\boldsymbol{x} \in \partial D_m \cap \partial D_d), \end{cases} \tag{6}$$

where there is no boundary condition on ∂D. This problem is separable in polar coordinates (r, θ) and admits even (resp. odd) solutions for any complex contrast κ that solves the even (resp. odd) dispersion relation

$$f_\phi^{\mathfrak{e}(\mathfrak{o})}(\eta, \kappa) := [1+\kappa] \sinh[\eta\pi] \underset{(+)}{-} [1-\kappa] \sinh[\eta(\pi-\phi)] = 0. \tag{7}$$

The proposition below summarizes this result, where the sets of zeros of these dispersion relations are denoted

$$H_\phi^{\mathfrak{e}(\mathfrak{o})}(\kappa) := \left\{\eta \in \mathbb{C} \;\middle|\; f_\phi^{\mathfrak{e}(\mathfrak{o})}(\eta, \kappa) = 0\right\},\ H_\phi(\kappa) := H_\phi^{\mathfrak{e}}(\kappa) \cup H_\phi^{\mathfrak{o}}(\kappa). \tag{8}$$

Proposition 2 (Local solutions). *Let $\phi \in (0, 2\pi)\backslash\{\pi\}$. For any $\kappa \in \mathbb{C}\backslash\{\kappa_\phi\}$, the solutions of the local transmission problem (6) with separated variables can be split into two families $\left(u_\eta^{\mathfrak{e}}\right)_{\eta \in H_\phi^{\mathfrak{e}}(\kappa)}$ and $\left(u_\eta^{\mathfrak{o}}\right)_{\eta \in H_\phi^{\mathfrak{o}}(\kappa)\backslash\{0\}}$ defined as*

$$u_\eta^{\mathfrak{e}(\mathfrak{o})}(r, \theta) := r^{i\eta} \times \Phi_\eta^{\mathfrak{e}(\mathfrak{o})}(\theta) \quad \left(\eta \in H_\phi^{\mathfrak{e}(\mathfrak{o})}(\kappa)\backslash\{0\}\right),\ u_0^{\mathfrak{e}}(r, \theta) := [1 + c\ln(r)] \times \Phi_0^{\mathfrak{e}}(\theta),$$

where the orthoradial functions $\Phi_\eta^{\mathfrak{e}}$ and $\Phi_\eta^{\mathfrak{o}}$ are given by (A.1) and (A.2), respectively.

Proof. Using weak derivatives, (6) reads

$$\operatorname{div}(\sigma\nabla u) = \frac{1}{r^2} r\partial_r(\sigma(\kappa,\theta) r \partial_r u) + \frac{1}{r^2}\partial_\theta(\sigma(\kappa,\theta)\partial_\theta u) = 0 \quad (r \in (0, R),\ \theta \in (-\pi, \pi]), \tag{9}$$

with $\sigma(\kappa, \theta) := \mathbb{1}_{\Theta_m}(\theta) + \kappa\, \mathbb{1}_{\Theta_d}(\theta)$. If we look for a solution with separated variables $u(r, \theta) = v(r)w(\theta)$ we get

$$\frac{1}{v(r)} r\partial_r(r\partial_r v(r)) = -\eta^2 = -\frac{1}{\sigma(\kappa,\theta)\, w(\theta)} \partial_\theta(\sigma(\kappa,\theta)\partial_\theta w(\theta)),$$

where $\eta \in \mathbb{C}$ is a seemingly free parameter. Proposition 22 shows that the orthoradial equation is solvable if and only if $f_\phi^{\mathfrak{e}}(\eta,\kappa) = 0$ or $f_\phi^{\mathfrak{o}}(\eta,\kappa) = 0$. Since $\kappa \neq \kappa_\phi$, the odd piecewise-linear function $\Phi_0^{\mathfrak{o}}$ cannot solve the orthoradial equation. The change of variables $z = \ln(r)$ enables to write the radial equation as $v''(z) = -\eta^2 v(z)$ on $(-\infty, \ln R)$, which is readily solvable for any $\eta \in \mathbb{C}$. □

The regularity of these local solutions at the corner is driven by the sign of $\Im(\eta)$:

- If $\Im(\eta) < 0$, then $u_\eta^{\mathfrak{e}(\mathfrak{o})}$ vanishes at the corner and $u_\eta^{\mathfrak{e}(\mathfrak{o})} \in H^1(D)$.
- If $\Im(\eta) > 0$ then $u_\eta^{\mathfrak{e}(\mathfrak{o})}$ blows up at $r = 0$ and $u_\eta^{\mathfrak{e}(\mathfrak{o})} \notin H^1(D)$.
- If $\Im(\eta) = 0$, then there are three cases to distinguish:
  - If $\eta \in \mathbb{R}^*$ then $u_\eta^{\mathfrak{e}(\mathfrak{o})}(r,\theta) = e^{i\eta \ln r}\Phi_\eta^{\mathfrak{e}(\mathfrak{o})}(\theta) \in L^2(D)\backslash H^1(D)$ is a strongly-oscillating function (in r) that does not have a limit at $r = 0$.
  - If $\eta = 0$ and $c = 0$, then $u_0^{\mathfrak{e}} \in H^1(D)$ since $u_0^{\mathfrak{e}}(r,\theta) = 1$.
  - If $\eta = 0$ and $c \neq 0$, then $u_0^{\mathfrak{e}} \in L^2(D)\backslash H^1(D)$ due to its logarithmic singularity.

Since we will use these local solutions to expand the solution of the PEP (1,2,3) in D, it will prove useful to know the content of $H_\phi(\kappa)$ for a given contrast κ and corner angle ϕ: Lemma 3 covers elementary properties while Proposition 4 covers the strongly-oscillating case $\eta \in \mathbb{R}^*$.

Lemma 3 (Elementary properties)**.** *Let $\kappa \in \mathbb{C}$ and $\phi \in (0, 2\pi)\backslash\{\pi\}$. The following properties hold:*

(a) $H_\phi^{\mathfrak{e}(\mathfrak{o})}(\kappa)$ *is countable and has no finite accumulation point.*

(b) *If $\eta \in H_\phi^{\mathfrak{e}(\mathfrak{o})}(\kappa)$, then $-\eta \in H_\phi^{\mathfrak{e}(\mathfrak{o})}(\kappa)$ and $\overline{\eta} \in H_\phi^{\mathfrak{e}(\mathfrak{o})}(\overline{\kappa})$.*

(c) $0 \in H_\phi^{\mathfrak{e}(\mathfrak{o})}(\kappa)$ *and* $H_\phi^{\mathfrak{e}}(\kappa) \cap H_\phi^{\mathfrak{o}}(\kappa) \subset i\mathbb{R}$.

Proof. See Appendix B.1. □

The next result shows that the strongly-oscillating case $\eta \in \mathbb{R}^*$ can only occur when κ belongs to the so-called *critical interval* I_c: [15, Eq. (10)]

$$I_c := I_c^{\mathfrak{o}} \cup I_c^{\mathfrak{e}},\ I_c^{\mathfrak{o}} := \begin{cases} (\kappa_\phi, -1) & (0 < \phi < \pi) \\ (-1, \kappa_\phi) & (\pi < \phi < 2\pi) \end{cases},\ I_c^{\mathfrak{e}} := \begin{cases} (-1, \kappa_\phi^{-1}) & (0 < \phi < \pi) \\ (\kappa_\phi^{-1}, -1) & (\pi < \phi < 2\pi) \end{cases}. \tag{10}$$

Proposition 4 (Critical interval)**.** *Let $\phi \in (0, 2\pi)\backslash\{\pi\}$. We have the equivalences*

$$\kappa \in I_c^{\mathfrak{e}(\mathfrak{o})} \Leftrightarrow H_\phi^{\mathfrak{e}(\mathfrak{o})}(\kappa) \cap \mathbb{R}^* \neq \varnothing \Leftrightarrow \exists!\, \eta_c > 0 :\ H_\phi^{\mathfrak{e}(\mathfrak{o})}(\kappa) \cap \mathbb{R}^* = \{\eta_c, -\eta_c\},$$

where the scalar η_c is the critical exponent*. Moreover, η_c crosses the real axis when κ crosses $I_c^{\mathfrak{e}(\mathfrak{o})}$.*

Proof. Let

$$\psi_\phi(\eta) := \frac{\sinh[\eta(\pi - \phi)]}{\sinh[\eta\pi]},\ \beta(x) := \frac{x-1}{x+1}. \tag{11}$$

The smooth even map ψ_ϕ is strictly monotonous on $(0, \infty)$, since $\psi_\phi'(\eta) = 0$ is equivalent to $a\tanh[\eta\pi] = \tanh[a\eta\pi]$ with $a = 1 - \phi/\pi$. ψ_ϕ maps $(0, \infty)$ onto $(\frac{\pi-\phi}{\pi}, 0)$ if $\phi \in (\pi, 2\pi)$ and onto $(0, \frac{\pi-\phi}{\pi})$ if $\phi \in (0, \pi)$. The claimed equivalences follow from $f_\phi^{\mathfrak{e}}(\eta,\kappa) = 0 \Leftrightarrow \kappa = \beta \circ \psi_\phi(\eta)$ and $f_\phi^{\mathfrak{o}}(\eta,\kappa) = 0 \Leftrightarrow 1/\kappa = \beta \circ \psi_\phi(\eta)$, where β is an increasing map from $(-1, 1)$ onto $(-\infty, 0)$. The last claim follows from the implicit function theorem and is proven in Appendix B.1. □

When the contrast is critical, i.e. when $\kappa \in I_c^{\mathfrak{e}(\mathfrak{o})}$, the two strongly-oscillating functions

$$u_{\eta_c}^{\mathfrak{e}(\mathfrak{o})}(r,\theta) = r^{i\eta_c}\Phi_{\eta_c}^{\mathfrak{e}(\mathfrak{o})}(\theta),\ u_{-\eta_c}^{\mathfrak{e}(\mathfrak{o})}(r,\theta) = r^{-i\eta_c}\Phi_{\eta_c}^{\mathfrak{e}(\mathfrak{o})}(\theta) = \overline{u_{\eta_c}^{\mathfrak{e}(\mathfrak{o})}}(r,\theta) \quad (r \in (0,R),\ \theta \in (-\pi,\pi]) \tag{12}$$

solve (6). These functions do not have a limit when $r \to 0$ and have vanishing phase velocities. As $\kappa \in I_c$ tends to κ_ϕ or $1/\kappa_\phi$, the (real) critical exponent η_c tends to 0, while as $\kappa \to -1$, η_c goes to infinity.

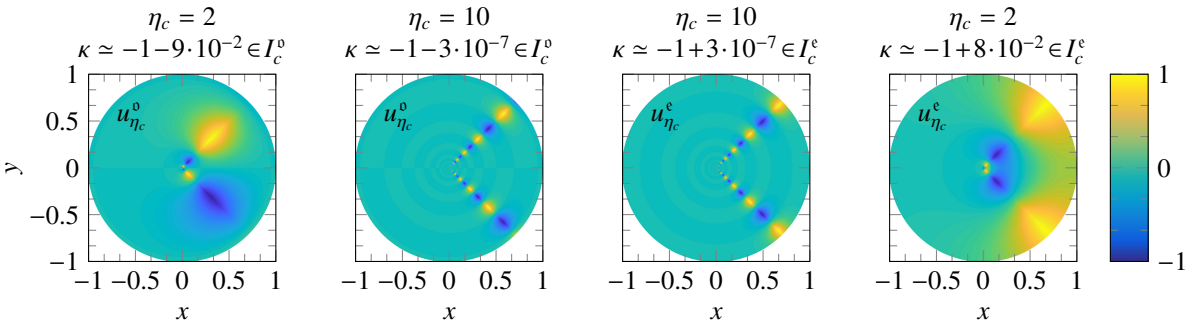

Fig. 2: Strongly-oscillating local solutions $\Re\left(u_{\eta_c}^{\mathfrak{e}(\mathfrak{o})}\right)/\|u_{\eta_c}^{\mathfrak{e}(\mathfrak{o})}\|_\infty$ given by (12) for a corner angle $\phi = \pi/2$. The contrast κ solves $f_\phi^{\mathfrak{e}(\mathfrak{o})}(\eta_c, \kappa) = 0$.

Remark 5. As $\phi \to \pi$ (locally flat interface), the closure of the critical interval reduces to $\{-1\}$. The closure of the critical interval can be interpreted as the essential spectrum of a suitably defined operator [13, 31, 14].

The results covered so far apply to any corner angle $\phi \neq \pi$ and constitute all that is needed to introduce complex plasmonic resonances in Section 2.2. The remainder of this section focuses on the case $\phi/\pi \in \mathbb{Q}$, for which the knowledge of H_ϕ is reduced to that of a bounded subset $\check{H}_\phi$ that can be obtained by solving a polynomial equation.

Proposition 6. *Let $\kappa \in \mathbb{C}\backslash\{-1\}$. If $\phi \in (0, 2\pi)\backslash\{\pi\}$ and $\phi/\pi = p/q$ with p and q coprime integers, then the set of zeros can be split into a κ-independent and a κ-dependent part:*

$$H_\phi^{\mathfrak{e}(\mathfrak{o})}(\kappa) = \left\{iq\mathbb{Z}\right\} \cup \left\{\check{H}_\phi^{\mathfrak{e}(\mathfrak{o})}(\kappa) + i2q\mathbb{Z}\right\}, \tag{13}$$

where $\check{H}_\phi^{\mathfrak{e}(\mathfrak{o})}(\kappa) \subset \{\eta \in \mathbb{C} \mid -q < \Im(\eta) \leq q\}$ contains at most $2(q-1)$ distinct elements and satisfies

$$\check{H}_\phi^{\mathfrak{e}}(\kappa) = \left\{\frac{q}{\pi}\ln(x) \;\middle|\; P_{\beta(\kappa)}^{(p,q)}(x) = 0\right\},\ \check{H}_\phi^{\mathfrak{o}}(\kappa) = \left\{\frac{q}{\pi}\ln(x) \;\middle|\; P_{-\beta(\kappa)}^{(p,q)}(x) = 0\right\},$$

where the polynomial $P_{\beta(\kappa)}^{(p,q)}$ is given by (B.1) and ln *denotes the principal branch of the logarithm.*

Proof. The proof consists in formulating a polynomial equation in $x = e^{\frac{\eta\pi}{q}}$, see Appendix B.2. □

For a right angle $\phi = \pi/2$, we have (see Example 24 for details)

$$\check{H}_\phi^{\mathfrak{e}}(\kappa) = \left\{\eta_{\beta(\kappa)}^+, -\eta_{\beta(\kappa)}^+\right\},\ \check{H}_\phi^{\mathfrak{o}}(\kappa) = \left\{\eta_{-\beta(\kappa)}^+, -\eta_{-\beta(\kappa)}^+\right\}, \tag{14}$$

where the zeros, which only depend on κ through $\beta(\kappa)$, are given by:

$$\eta_{\beta(\kappa)}^+ := \frac{2}{\pi}\ln\left[\frac{-\beta(\kappa) + \sqrt{\beta(\kappa)^2 - 4}}{2}\right],\ \eta_{-\beta(\kappa)}^+ := \frac{2}{\pi}\ln\left[\frac{\beta(\kappa) + \sqrt{\beta(\kappa)^2 - 4}}{2}\right], \tag{15}$$

using the principal branches of both ln and $\sqrt{\cdot}$. In agreement with Proposition 4, we have:

$$\kappa \in I_c^{\mathfrak{e}} = (-1, -1/3) \Leftrightarrow \beta(\kappa) \in (-\infty, -2) \Leftrightarrow \eta_{\beta(\kappa)}^+(\kappa) > 0,\ \kappa \in I_c^{\mathfrak{o}} = (-3, -1) \Leftrightarrow \beta(\kappa) \in (2, +\infty) \Leftrightarrow \eta_{-\beta(\kappa)}^+(\kappa) > 0.$$

The associated strongly-oscillating local solutions are plotted in Figure 2. The case $\phi = \pi/3$ is similar:

$$\check{H}_\phi^{\mathfrak{e}}(\kappa) = \left\{\eta_{\beta(\kappa)}^{+,+}, \eta_{\beta(\kappa)}^{+,-}, -\eta_{\beta(\kappa)}^{+,+}, -\eta_{\beta(\kappa)}^{+,-}\right\},\ \check{H}_\phi^{\mathfrak{o}}(\kappa) = \left\{\eta_{-\beta(\kappa)}^{+,+}, \eta_{-\beta(\kappa)}^{+,-}, -\eta_{-\beta(\kappa)}^{+,+}, -\eta_{-\beta(\kappa)}^{+,-}\right\},$$

see Example 25 for details. Using these results Figure 3 plots the zeros for $\phi = \pi/2$ and $\phi = \pi/3$, highlighting the structure (13). It also shows the two real critical exponents $\pm\eta_c$ that are obtained when $\kappa \in I_c$.

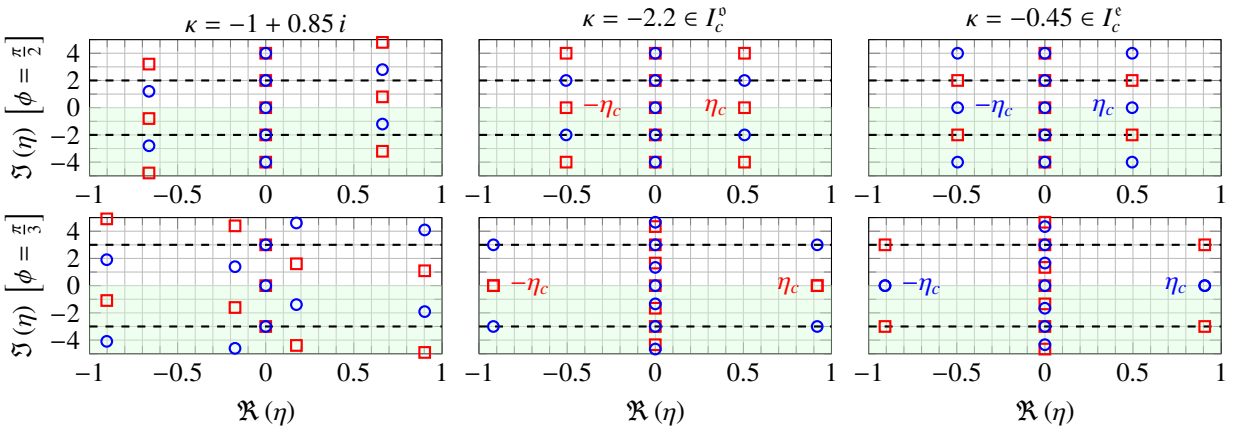

Fig. 3: Sets of zeros, computed using Proposition 6. (○): $H_\phi^{\mathfrak{e}}(\kappa)$, (□): $H_\phi^{\mathfrak{o}}(\kappa)$. The stable region $\{\Im(\eta) < 0\}$ is shaded. (Top row) $\phi = \pi/2$, for which $\check{H}_\phi^{\mathfrak{e}(\mathfrak{o})}(\kappa) \subset \{\eta \in \mathbb{C} \,|\, -2 < \Im(\eta) \leq 2\}$. (Bottom row) $\phi = \pi/3$, for which $\check{H}_\phi^{\mathfrak{e}(\mathfrak{o})}(\kappa) \subset \{\eta \in \mathbb{C} \,|\, -3 < \Im(\eta) \leq 3\}$.

2.2. *From multivalued zeros to complex plasmonic resonances*

We denote by $\mathbb{C}^+$ and $\mathbb{C}^-$ the open upper and lower half-spaces

$$\mathbb{C}^+ := \{z \in \mathbb{C} \,|\, \Im(z) > 0\}\,, \quad \mathbb{C}^- := \{z \in \mathbb{C} \,|\, \Im(z) < 0\}\,.$$

Let $\kappa_0 \in \mathbb{C}^+$ and u be a $H^1(D)$ solution of the local transmission problem (6) with $\kappa = \kappa_0$. From the properties gathered in Section 2.1, notably the discussion that followed Proposition 2, u admits the asymptotic expansion

$$u(r,\theta) \underset{r\to 0}{=} c_0 + \sum_{\substack{\eta \in \widetilde{H}_\phi^{\mathfrak{e}}(\kappa_0) \\ \eta_\star < \Im(\eta)}} c_\eta^{\mathfrak{e}}\, r^{i\eta} \Phi_\eta^{\mathfrak{e}}(\theta) + \sum_{\substack{\eta \in \widetilde{H}_\phi^{\mathfrak{o}}(\kappa_0) \\ \eta_\star < \Im(\eta)}} c_\eta^{\mathfrak{o}}\, r^{i\eta} \Phi_\eta^{\mathfrak{o}}(\theta) + O\left(r^{-\eta_\star}\right) \quad (r \in (0,R),\ \theta \in (-\pi,\pi]), \tag{16}$$

for any $\eta_\star < 0$, where the sets of so-called *stable zeros* of the dispersion relations are defined for any $\kappa \in \mathbb{C}^+$ as

$$\widehat{H}_\phi^{\mathfrak{e}(\mathfrak{o})}(\kappa) := \left\{\eta \in H_\phi^{\mathfrak{e}(\mathfrak{o})}(\kappa) \,\middle|\, \Im(\eta) < 0\right\},\ \widehat{H}_\phi(\kappa) := \widehat{H}_\phi^{\mathfrak{e}}(\kappa) \cup \widehat{H}_\phi^{\mathfrak{o}}(\kappa) \quad (\kappa \in \mathbb{C}^+)\,. \tag{17}$$

A rigorous derivation of (16) could be carried out by inverting the Mellin transform of u using the residue theorem, see [38, § 3.5] as well as [39, § 1.2] [40, Chap. 2] [41, § 2] [42, Chap. 2].

The purpose of this section is to construct a definition of complex plasmonic resonances by continuing $\kappa \mapsto \widehat{H}_\phi(\kappa)$, well-defined for any $\kappa \in \mathbb{C}^+$, to $\mathbb{C}^-$. The construction proceeds in three steps. Section 2.2.1 shows that $\widehat{H}_\phi$ has three branch points given by $\kappa = \kappa_\phi$, $\kappa = 1/\kappa_\phi$, and $\kappa = -1$. Section 2.2.2 introduces three different analytic continuations to $\mathbb{C}^-$, depending on where κ crosses the real axis. This leads in Section 2.2.3 to the definition of distinct families of contrasts: isolated plasmonic eigenvalues, embedded plasmonic eigenvalues, and complex plasmonic resonances.

2.2.1. *Branch points of the set of stable zeros*

Before tackling the general case it is instructive to highlight the multivalued nature of the set of stable zeros $\widehat{H}_\phi^{\mathfrak{e}(\mathfrak{o})}$ when $\phi = \pi/2$, since for this corner angle the zeros are known in closed form (13,14,15).

Example 7 (Case $\phi = \pi/2$)**.** The zero $\eta^+_{-\beta(\kappa)}$ is null only for $\kappa = -3$ ($\beta(\kappa) = 2$) and is singular only at $\kappa = -1$ ($|\beta(\kappa)| = \infty$). These two values are in fact algebraic and logarithmic branch points, respectively:

$$\eta^+_{-\beta(\kappa)} \underset{\kappa\to -3}{=} \frac{2}{\pi}\sqrt{\beta(\kappa)-2} + O\left(|\beta(\kappa)-2|\right),\ \exp\left(\eta^+_{-\beta(\kappa)}\frac{\pi}{2}\right) \underset{\kappa\to -1}{=} \beta(\kappa) - \frac{1}{\beta(\kappa)} + O\left(\frac{1}{|\beta(\kappa)|^3}\right).$$

When κ circles *once* around -3, $\beta(\kappa)$ loops around 2 and the zeros $\eta^+_{-\beta(\kappa)}$ and $-\eta^+_{-\beta(\kappa)}$ swap places, each crossing the real axis *once*. When κ circles *once* around -1, $\eta^+_{-\beta(\kappa)}$ gets translated by $(i2\pi) \times \frac{2}{\pi} = i4$ or $-i4$, depending on the direction of rotation. Let us now see what this implies for the sets of zeros defined so far:

- Let $\kappa \in \mathbb{C}\backslash\{-1\}$. The set $\breve{H}^{\mathfrak{o}}_{\phi}(\kappa) + i4\mathbb{Z}$ contains all the possible values for $\eta^{+}_{-\beta(\kappa)}$ and $-\eta^{+}_{-\beta(\kappa)}$, so the map $\kappa \mapsto \breve{H}^{\mathfrak{o}}_{\phi}(\kappa) + i4\mathbb{Z}$ is not multivalued. A fortiori, the map $\kappa \mapsto H^{\mathfrak{o}}_{\phi}(\kappa)$ is not multivalued. See (13).
- Let $\kappa \in \mathbb{C}^{+}$. The set $\widehat{H}^{\mathfrak{o}}_{\phi}(\kappa)$ contains either $\eta^{+}_{-\beta(\kappa)}$ or $-\eta^{+}_{-\beta(\kappa)}$ but not both, so $\kappa = -3$ is an algebraic branch point of $\kappa \mapsto \widehat{H}^{\mathfrak{o}}_{\phi}(\kappa)$. Moreover, $\widehat{H}^{\mathfrak{o}}_{\phi}(\kappa)$ does not contain $\eta^{+}_{-\beta(\kappa)} + i4$ or $-\eta^{+}_{-\beta(\kappa)} + i4$ (since they have positive imaginary parts), so $\kappa = -1$ is a logarithmic branch point of $\kappa \mapsto \widehat{H}^{\mathfrak{o}}_{\phi}(\kappa)$.

The even case is deduced with the substitution $(\beta(\kappa), -3, \mathfrak{o}) \to (-\beta(\kappa), -1/3, \mathfrak{e})$.

In the general case no closed form expression is available for the zeros. However the next result shows that if $\kappa \notin \{\kappa_\phi, 1/\kappa_\phi\}$, then $H^{\mathfrak{e}(\mathfrak{o})}_{\phi}(\kappa)$ consists only of simple zeros that depend analytically on κ.

Proposition 8. *Let $\phi \in (0, 2\pi)\backslash\{\pi\}$ and $\kappa_0 \in U \coloneqq \mathbb{C}\backslash\{\kappa_\phi, 1/\kappa_\phi\}$. For any $\eta_0 \in H^{\mathfrak{e}(\mathfrak{o})}_{\phi}(\kappa_0)$, there are a neighborhood $V \subset U$ of κ_0 and a unique analytic map $\tilde{\eta} : V \to \mathbb{C}$ such that $\tilde{\eta}(\kappa_0) = \eta_0$ and $\tilde{\eta}(\kappa) \in H^{\mathfrak{e}(\mathfrak{o})}_{\phi}(\kappa)$ for any $\kappa \in V$.*

Proof. Consequence of the implicit function theorem [43, Prop. 2.14], see Appendix B.1. □

Note that the above proposition does apply to $\kappa = -1$, as $H^{\mathfrak{e}(\mathfrak{o})}_{\phi}(-1) = i\frac{\pi}{\pi-\phi}\mathbb{Z}$ is well-defined. However, the value $\kappa = -1$ is a singularity in the sense that some elements of $H^{\mathfrak{e}(\mathfrak{o})}_{\phi}(\kappa)$ go to infinity when $\kappa \to -1$ (e.g. the critical exponent η_c). Therefore from now on the map $\kappa \mapsto H^{\mathfrak{e}(\mathfrak{o})}_{\phi}(\kappa)$ is always considered defined on the open subset

$$K \coloneqq \mathbb{C}\backslash\left\{\kappa_\phi, \frac{1}{\kappa_\phi}, -1\right\}.$$

Although the map $\kappa \mapsto H^{\mathfrak{e}(\mathfrak{o})}_{\phi}(\kappa)$ is single-valued, we have the following result.

Proposition 9. *Let $\phi \in (0, 2\pi)\backslash\{\pi\}$. The map $\mathbb{C}^{+} \ni \kappa \mapsto \widehat{H}^{\mathfrak{e}(\mathfrak{o})}_{\phi}(\kappa)$ defined by (17) has one algebraic branch point at $\kappa = 1/\kappa_\phi$ (resp. $\kappa = \kappa_\phi$) and one logarithmic branch point at $\kappa = -1$.*

Proof. Follows from asymptotic expansions of the critical exponent, as in Example 7, see Appendix B.1. □

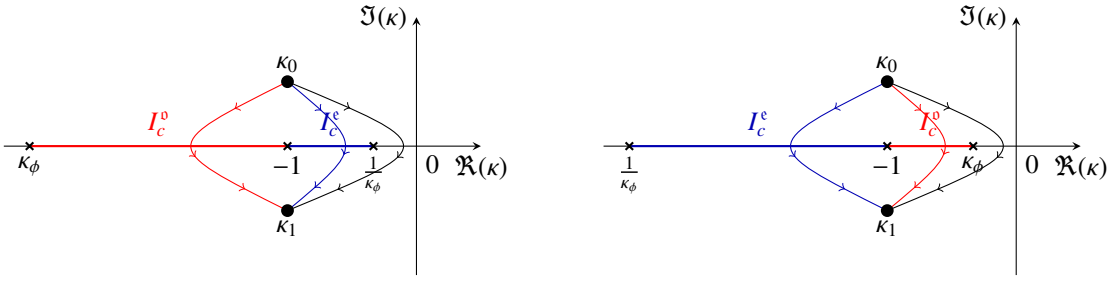

(a) $0 < \phi < \pi$. (b) $\pi < \phi < 2\pi$.

Fig. 4: Complex paths satisfying (18), each crossing the real axis at a different location: Γ_ϕ crosses outside the closure of the critical interval $\overline{I_c}$, $\Gamma^{\mathfrak{e}}_{\phi}$ crosses through $I^{\mathfrak{e}}_c$, and $\Gamma^{\mathfrak{o}}_{\phi}$ crosses through $I^{\mathfrak{o}}_c$.

2.2.2. *Analytic continuations of the set of stable zeros*

Intuitively, we would like to track the elements of $\widehat{H}_\phi(\kappa)$ as κ travels from $\kappa_0 \in \mathbb{C}^{+}$ to the lower half-plane $\mathbb{C}^{-}$. To achieve this, we define a smooth complex path Γ that satisfies

$$\Gamma : (0, 1) \to \mathbb{C}, \ \Gamma(0) = \kappa_0, \ \Gamma(1) = \kappa_1, \tag{18}$$

where κ_1 is an arbitrary contrast in $\mathbb{C}^{-}$. Proposition 8 implies that each element of $H_\phi(\kappa_0)$ can be considered as an analytic map defined in some neighborhood of κ_0; "tracking" an element of $H_\phi(\kappa_0)$ means building the analytic continuation of this map along Γ. Figure 4 sketches the three paths considered, which differ by where the real axis is crossed: Γ_ϕ crosses the real axis outside the closure of the critical interval $\overline{I_c}$, while $\Gamma^{\mathfrak{e}}_{\phi}$ (resp. $\Gamma^{\mathfrak{o}}_{\phi}$) crosses the real axis through the even (resp. odd) critical interval $I^{\mathfrak{e}}_c$ (resp. $I^{\mathfrak{o}}_c$). The top graph of Figure 5 plots $\widehat{H}_\phi(\kappa_0)$ for $\phi = \pi/2$.

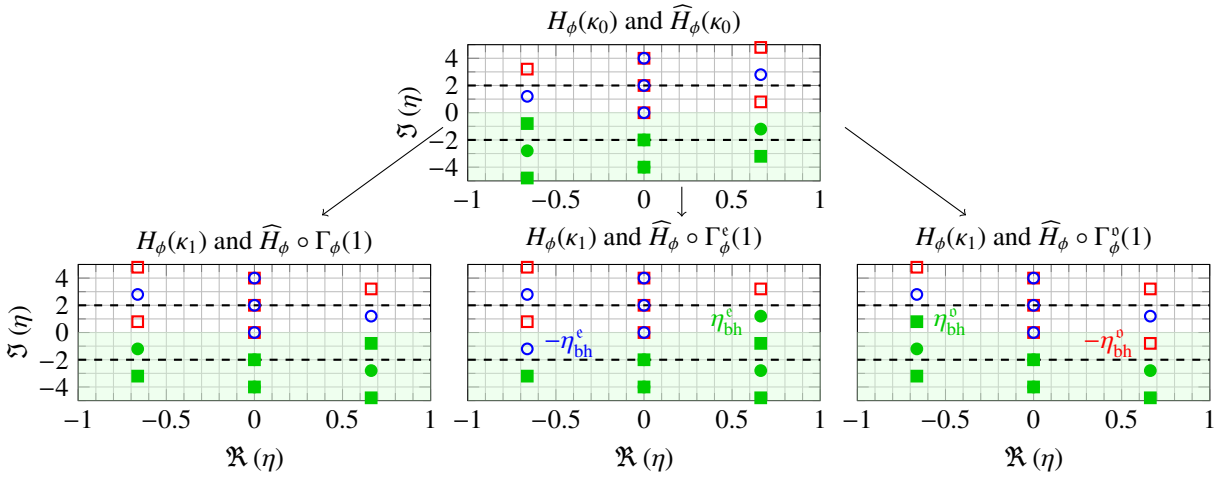

Fig. 5: Analytic continuation of $\kappa \mapsto \widehat{H}_\phi(\kappa)$ along each path of Figure 4, with $\phi = \pi/2$, $\kappa_0 = -1 + 0.85\,i \in \mathbb{C}^+$, and $\kappa_1 = \overline{\kappa_0}$. (○,●): $H^{\mathrm{e}}_\phi(\kappa)$, (□,■): $H^{\mathrm{o}}_\phi(\kappa)$. (Top) (●,■): $\widehat{H}_\phi(\kappa_0)$ given by (17). (Bottom left) (●,■): $\widehat{H}_\phi \circ \Gamma_\phi(1)$ given by (19) (no zero has crossed $\mathbb{R}$). (Bottom center) (●,■): $\widehat{H}_\phi \circ \Gamma^{\mathrm{e}}_\phi(1)$ given by (21) (the pair $\pm\eta^{\mathrm{e}}_{\mathrm{bh}}$ has crossed $\mathbb{R}$). (Bottom right) (●,■): $\widehat{H}_\phi \circ \Gamma^{\mathrm{o}}_\phi(1)$ given by (23) (the pair $\pm\eta^{\mathrm{o}}_{\mathrm{bh}}$ has crossed $\mathbb{R}$).

Crossing through $\mathbb{R}\backslash\overline{I_c}$. Let us first consider the behavior of $\widehat{H}_\phi$ along Γ_ϕ. Proposition 4 gives that for any $s \in [0,1]$, $\widehat{H}_\phi \circ \Gamma_\phi(s)$ never contains a real element. In other words, no element of $\widehat{H}_\phi(\kappa)$ crosses the real axis as κ travels along Γ_ϕ. This provides us with a first value for "$\widehat{H}_\phi(\kappa_1)$", namely

$$\widehat{H}_\phi \circ \Gamma_\phi(1) = \left\{\eta \in H_\phi(\kappa_1) \,\middle|\, \Im(\eta) < 0\right\}, \tag{19}$$

which is the one we could have expected at first sight. The bottom left graph of Figure 5 plots $\widehat{H}_\phi \circ \Gamma_\phi(1)$.

Crossing through I^{e}_c. The main difference between Γ_ϕ and the even-crossing path Γ^{e}_ϕ follows from Proposition 4: when $\Gamma^{\mathrm{e}}_\phi(s)$ reaches I^{e}_c coming from $\mathbb{C}^+$, two non-null elements of $H^{\mathrm{e}}_\phi \circ \Gamma^{\mathrm{e}}_\phi(s)$ become real, namely $\pm\eta_c$. One of them, defined as the *black-hole* zero $\eta^{\mathrm{e}}_{\mathrm{bh}}$, comes from the stable region $\mathbb{C}^-$ while the other one comes from the unstable region $\mathbb{C}^+$. By contrast, no elements of $\widehat{H}^{\mathrm{o}}_\phi \circ \Gamma^{\mathrm{e}}_\phi$ become real. The link between $\eta^{\mathrm{e}}_{\mathrm{bh}}$ and η_c depends upon the corner angle ϕ: [15, Tab. 1]

$$\forall \kappa \in I^{\mathrm{e}}_c,\ \eta^{\mathrm{e}}_{\mathrm{bh}}(\kappa) \coloneqq +\eta_c > 0 \quad (0 < \phi < \pi)\,,\ \eta^{\mathrm{e}}_{\mathrm{bh}}(\kappa) \coloneqq -\eta_c < 0 \quad (\pi < \phi < 2\pi)\,. \tag{20}$$

As $\Gamma^{\mathrm{e}}_\phi(s)$ leaves I^{e}_c to enter $\mathbb{C}^-$, the black-hole zero $\eta^{\mathrm{e}}_{\mathrm{bh}}$ crosses $\mathbb{R}$ towards the unstable region $\mathbb{C}^+$ while $-\eta^{\mathrm{e}}_{\mathrm{bh}}$ crosses $\mathbb{R}$ towards the stable region $\mathbb{C}^-$. Eventually κ_1 is reached and we arrive at a second value for "$\widehat{H}_\phi(\kappa_1)$":

$$\widehat{H}_\phi \circ \Gamma^{\mathrm{e}}_\phi(1) = \left\{\eta \in H_\phi(\kappa_1) \,\middle|\, \Im(\eta) < 0,\ \eta \neq -\eta^{\mathrm{e}}_{\mathrm{bh}}(\kappa_1)\right\} \cup \left\{\eta^{\mathrm{e}}_{\mathrm{bh}}(\kappa_1)\right\}, \tag{21}$$

which is shown in the bottom center plot of Figure 5 (compare with the bottom left plot).

Remark 10 (Definition of the black-hole zero). Let us emphasize the mathematical meaning of (20). For any $\kappa \in I^{\mathrm{e}}_c$, η_c is a scalar uniquely defined in Proposition 4 and Proposition 8 provides us with an analytic map $\tilde{\eta}_c : V \subset U \to \mathbb{C}$ such that $\tilde{\eta}_c(\kappa) = \eta_c$. The black-hole zero $\eta^{\mathrm{e}}_{\mathrm{bh}}$ is then *defined* as the analytic continuation along Γ^{e}_ϕ of $\tilde{\eta}_c$ (if $\phi \in (0,\pi)$) or $-\tilde{\eta}_c$ (if $\phi \in (\pi, 2\pi)$).

Crossing through I^{o}_c. Since Proposition 4 applies to both the odd and even cases, the odd-crossing path leads to a similar phenomenon. The only difference is that the black-hole zero belongs to H^{o}_ϕ and has the sign [15, Tab. 1]

$$\forall \kappa \in I^{\mathrm{o}}_c,\ \eta^{\mathrm{o}}_{\mathrm{bh}}(\kappa) \coloneqq -\eta_c < 0 \quad (0 < \phi < \pi)\,,\ \eta^{\mathrm{o}}_{\mathrm{bh}}(\kappa) \coloneqq +\eta_c > 0 \quad (\pi < \phi < 2\pi)\,, \tag{22}$$

which leads to a third value for "$\widehat{H}_\phi(\kappa_1)$":

$$\widehat{H}_\phi \circ \Gamma^{\mathrm{o}}_\phi(1) = \left\{\eta \in H_\phi(\kappa_1) \,\middle|\, \Im(\eta) < 0,\ \eta \neq -\eta^{\mathrm{o}}_{\mathrm{bh}}(\kappa_1)\right\} \cup \left\{\eta^{\mathrm{o}}_{\mathrm{bh}}(\kappa_1)\right\}, \tag{23}$$

plotted in the bottom right graph of Figure 5.

Summary. Starting from a contrast κ_0 in the upper half-plane we have obtained three different values for "$\widehat{H}_\phi(\kappa_1)$", depending on where the real axis has been crossed. To summarize, let us explicitly write down the three corresponding analytic continuations of $\widehat{H}_\phi$. The continuation across $\mathbb{R}\backslash\overline{I_c}$ is given by

$$\widehat{H}_\phi(\kappa) := \widehat{H}^{\mathfrak{e}}_\phi(\kappa) \cup \widehat{H}^{\mathfrak{o}}_\phi(\kappa) \qquad \left(\kappa \in \mathbb{C}^+ \cup \left[\mathbb{R}\backslash\overline{I_c}\right] \cup \mathbb{C}^-\right) \tag{24}$$

and the continuations across $I_c^{\mathfrak{e}}$ and $I_c^{\mathfrak{o}}$ are given by

$$\widehat{H}^{|\mathfrak{e}}_\phi(\kappa) := \widehat{H}^{\mathfrak{e}|\mathfrak{e}}_\phi(\kappa) \cup \widehat{H}^{\mathfrak{o}}_\phi(\kappa) \ \ (\kappa \in \mathbb{C}^+ \cup I_c^{\mathfrak{e}} \cup \mathbb{C}^-)\,, \ \widehat{H}^{|\mathfrak{o}}_\phi(\kappa) := \widehat{H}^{\mathfrak{e}}_\phi(\kappa) \cup \widehat{H}^{\mathfrak{o}|\mathfrak{o}}_\phi(\kappa) \ \ (\kappa \in \mathbb{C}^+ \cup I_c^{\mathfrak{o}} \cup \mathbb{C}^-)\,, \tag{25}$$

where

$$\begin{aligned}
&\widehat{H}^{\mathfrak{e}(\mathfrak{o})}_\phi(\kappa) := \left\{\eta \in H^{\mathfrak{e}(\mathfrak{o})}_\phi(\kappa) \,\middle|\, \Im(\eta) < 0\right\} && \left(\kappa \in \mathbb{C}^+ \cup \left[\mathbb{R}\backslash\overline{I_c^{\mathfrak{e}(\mathfrak{o})}}\right] \cup \mathbb{C}^-\right)\\
&\widehat{H}^{\mathfrak{e}(\mathfrak{o})|\mathfrak{e}(\mathfrak{o})}_\phi := \left\{\eta \in H^{\mathfrak{e}(\mathfrak{o})}_\phi(\kappa) \,\middle|\, \Im(\eta) < 0,\ \eta \neq -\eta^{\mathfrak{e}(\mathfrak{o})}_{\mathrm{bh}}(\kappa)\right\} \cup \left\{\eta^{\mathfrak{e}(\mathfrak{o})}_{\mathrm{bh}}(\kappa)\right\} && \left(\kappa \in \mathbb{C}^+ \cup I_c^{\mathfrak{e}(\mathfrak{o})} \cup \mathbb{C}^-\right).
\end{aligned}$$

By construction the sets $\widehat{H}_\phi(\kappa)$, $\widehat{H}^{|\mathfrak{e}}_\phi(\kappa)$, and $\widehat{H}^{|\mathfrak{o}}_\phi(\kappa)$ are identical for $\kappa \in \mathbb{C}^+$ but differ elsewhere. For any $\kappa \in \mathbb{C}^-$, $\widehat{H}_\phi(\kappa) \subset \mathbb{C}^-$ while $\widehat{H}^{|\mathfrak{e}(\mathfrak{o})}_\phi(\kappa)$ contains the unstable black-hole zero $\eta^{\mathfrak{e}(\mathfrak{o})}_{\mathrm{bh}}(\kappa) \in \mathbb{C}^+$, see the bottom row of Figure 5.

2.2.3. *Definition of complex plasmonic resonances*

Section 2.2.2 has defined three analytic continuations to $\mathbb{C}^-$ of the set of stable zeros (17), namely $\widehat{H}_\phi(\kappa)$ given by (24) and $\widehat{H}^{|\mathfrak{e}(\mathfrak{o})}_\phi(\kappa)$ given by (25). Each one leads below to the definition of a family of contrasts. Let us begin by defining isolated plasmonic eigenvalues.

Definition 11 (Isolated plasmonic eigenvalue)**.** A contrast κ is an *isolated plasmonic (IP) eigenvalue* if $\kappa \in (-\infty, 0]\backslash\overline{I_c}$ and there is u such that (u, κ) solves the PEP (1,2,3) and satisfies: for any $\eta_\star < 0$,

$$u(r,\theta) \underset{r\to 0}{=} c_0 + \sum_{\substack{\eta\in\widehat{H}^{\mathfrak{e}}_\phi(\kappa)\\ \eta_\star<\Im(\eta)}} c^{\mathfrak{e}}_\eta\, r^{i\eta}\Phi^{\mathfrak{e}}_\eta(\theta) + \sum_{\substack{\eta\in\widehat{H}^{\mathfrak{o}}_\phi(\kappa)\\ \eta_\star<\Im(\eta)}} c^{\mathfrak{o}}_\eta\, r^{i\eta}\Phi^{\mathfrak{o}}_\eta(\theta) + O\left(r^{-\eta_\star}\right) \quad (r \in (0,R),\ \theta \in (-\pi,\pi]). \tag{26}$$

These "usual" eigenvalues can be computed without any specific treatment of the corner; the associated eigenfunctions belong to $H^1_{\mathrm{loc}}(\mathbb{R}^2)$ and are surface plasmons. If κ belongs to or crosses $I_c^{\mathfrak{e}(\mathfrak{o})}$ then the local expansion (26) must be against the continuation $\widehat{H}^{|\mathfrak{e}(\mathfrak{o})}_\phi(\kappa)$ and not $\widehat{H}_\phi(\kappa)$, which leads to the definitions of embedded plasmonic eigenvalues and complex plasmonic resonances below (the odd variants are obtained by swapping "$\mathfrak{e}$" and "$\mathfrak{o}$").

Definition 12 (Embedded plasmonic eigenvalue)**.** An *even-critical embedded plasmonic (EP) eigenvalue* is a real contrast $\kappa \in I_c^{\mathfrak{e}}$ for which there is u such that (u, κ) solves the PEP (1,2,3) and satisfies: for any $\eta_\star < 0$,

$$u(r,\theta) \underset{r\to 0}{=} c_0 + \sum_{\substack{\eta\in\widehat{H}^{\mathfrak{e}|\mathfrak{e}}_\phi(\kappa)\\ \eta_\star<\Im(\eta)}} c^{\mathfrak{e}}_\eta\, r^{i\eta}\Phi^{\mathfrak{e}}_\eta(\theta) + \sum_{\substack{\eta\in\widehat{H}^{\mathfrak{o}}_\phi(\kappa)\\ \eta_\star<\Im(\eta)}} c^{\mathfrak{o}}_\eta\, r^{i\eta}\Phi^{\mathfrak{o}}_\eta(\theta) + O\left(r^{-\eta_\star}\right) \quad (r \in (0,R),\ \theta \in (-\pi,\pi]) \tag{27}$$

with $c^{\mathfrak{e}}_{\eta^{\mathfrak{e}}_{\mathrm{bh}}} = 0$.

Similarly to IP eigenvalues, the associated eigenfunctions belong to $H^1_{\mathrm{loc}}(\mathbb{R}^2)$, since $c^{\mathfrak{e}}_{\eta^{\mathfrak{e}}_{\mathrm{bh}}} = 0$, and are surface plasmons. [35, Thm. 8] shows that given a symmetric particle Ω_m with a C^2 boundary there exists a corner perturbation that generates EP eigenvalues. Since the PEP is self-adjoint its eigenvalues must be real; complex resonances are intrinsic entities that do not belong to the spectrum: to obtain them, we must cross the critical interval.

Definition 13 (Complex plasmonic resonance)**.** An *even-critical complex plasmonic (CP) resonance* is a complex contrast $\kappa \in \mathbb{C}^-$ for which there is u such that (u, κ) solves the PEP (1,2,3) and satisfies (27) for any $\eta_\star < 0$.

If κ is an even-critical CP resonance then necessarily $c^{\mathfrak{e}}_{\eta^{\mathfrak{e}}_{\mathrm{bh}}} \neq 0$ so that the associated CP resonance function is a surface plasmon that blows up at the corner like

$$u(r,\theta) \underset{r\to 0}{=} c_0 + c^{\mathfrak{e}}_{\eta^{\mathfrak{e}}_{\mathrm{bh}}}\, r^{i\eta^{\mathfrak{e}}_{\mathrm{bh}}}\Phi^{\mathfrak{e}}_{\eta^{\mathfrak{e}}_{\mathrm{bh}}}(\theta) + O\left(|r^{i\eta}|\right) \underset{r\to 0}{\sim} r^{i\eta^{\mathfrak{e}}_{\mathrm{bh}}} \quad \left(\eta^{\mathfrak{e}}_{\mathrm{bh}} \in \mathbb{C}^+, \eta \in \mathbb{C}^-\right). \tag{28}$$

The existence of CP resonances will be investigated numerically in Section 5. In contrast with IP eigenvalues, the computation of both EP eigenvalues and CP resonances requires a particular treatment of the corner. In this work, we will use a corner complex scaling, first introduced in [15] to solve the plasmonic scattering problem with $\kappa \in I_c$. The applicability of this technique to our present endeavor is the subject of the next section.

Remark 14. Initially taking κ_0 in $\mathbb{C}^-$ would lead to conjugated definitions. This follows from Lemma 3(b).

Remark 15. The logarithmic singularity in r associated with $\eta = 0$ (see Proposition 2) is absent from (27). This can be justified by noting that $0 \in H^s_\phi(\kappa)$ for *any* $\kappa \in \mathbb{C}$. Therefore, this singularity cannot arise during the analytic continuation of a solution $u \in H^1_{\text{loc}}(\mathbb{R}^2)$ of the PEP (1,2,3) with $\kappa = \kappa_0 \in \mathbb{C}^+$: if this singularity was present at *one* contrast value then it would be present at *all* contrast values, contradicting the fact that $u \in H^1_{\text{loc}}(\mathbb{R}^2)$.

3. Definition and analysis of corner complex scaling

This section focuses on the computational technique that will be used to compute CP resonances, namely the corner complex scaling first introduced in [15]. Section 3.1 formulates the complex-scaled PEP in Definition 16. Section 3.2 shows that the eigenvalues of the complex-scaled PEP that lie inside the so-called uncovered region are CP resonances or EP eigenvalues. The dependence upon the scaling parameter of the uncovered region is studied, in preparation for the numerical investigations carried out in Sections 4 and 5.

3.1. Definition of corner complex scaling

By definition a CP resonance function blows up at the corner like (28), so the associated CP resonance κ cannot be an L^2 eigenvalue of the PEP (1,2,3). Mathematically, the PEP can be written as a self-adjoint eigenvalue problem in L^2 so its spectrum must be real-valued. Numerically, a FE discretization of the PEP yields a Hermitian generalized eigenvalue problem. The general principle of complex scaling is to define a *non* self-adjoint complex-scaled PEP that relies on a scaling parameter $\alpha \in \mathbb{C}$, which we denote PEPα, such that some L^2 eigenvalues of the PEPα turn out to be CP resonances of the original PEP.

The origin of complex scaling is typically traced back to [44] and [45], where it is used to compute scattering resonances of the Hamiltonian operator [46, Chap. 16]. In these works, the complex-scaling method can be understood as consisting in surrounding the scatterer by an absorbing layer that does not induce spurious reflections: as such, it is similar to the time-harmonic variant of the PML method, first proposed on physical grounds in [47] for electromagnetic waves in the time domain. The link between the PML and complex-scaling methods has been highlighted early, see [48] and [49] where "coordinate stretching" and "coordinate mapping" methods are discussed in the context of the PML method. For an analysis of the computation of scattering resonances using a PML, see [50] and [51, § 2.7]. Applications in fluid mechanics and acoustics can be found in e.g. [52] and [53]. In the remainder of this paper we will rely on a variant of complex scaling where the scaling is applied not at infinity, as in the works quoted above, but at the corner of the particle Ω_m. This scaling has been introduced in [15], where it is used to solve the plasmonic scattering problem with a critical contrast (i.e. $\kappa \in I_c$).

Since CP resonance functions are singular solely at the corner, the PEP and the PEPα need only differ in a neighborhood of the corner. Let us consider the neighborhood D depicted in Figure 1b, where (1,2) reduces to (9). The intuition behind the definition of the complex-scaled eigenproblem is as follows: if κ is a CP resonance, associated with a CP resonance function that blows up like

$$u(r,\theta) \underset{r\to 0}{\sim} r^{i\eta}$$

for some $\eta \in \mathbb{C}^+$, we would like κ to be associated with an eigenfunction of the PEPα that satisfies

$$u_\alpha(r,\theta) \underset{r\to 0}{=} c_0 + O\left(r^{i\frac{\eta}{\alpha}}\right),$$

where α is a scaling parameter *chosen* so that $r^{i\frac{\eta}{\alpha}}$ vanishes at the corner, i.e. $\Im(\eta/\alpha) < 0$. This can be achieved through the substitution "$r\partial_r \to \alpha r\partial_r$" in (9), which leads to the following definition of the PEPα, where Δ_α denotes the radially-scaled Laplacian:

$$\Delta_\alpha u(r,\theta) := \frac{1}{r^2}\alpha r\partial_r\left(\alpha r\partial_r u\right)(r,\theta) + \frac{1}{r^2}\partial_\theta\left(\partial_\theta u\right)(r,\theta). \tag{29}$$

Definition 16 (Complex-scaled PEP)**.** Let $\alpha \in \mathbb{C}\backslash\{0\}$ and $D_\alpha := \{|\boldsymbol{x} - \boldsymbol{x}_c| < R_\alpha\}$ with $R_\alpha \leq R$, as depicted in Figure 6. The complex-scaled PEP, denoted PEPα, is: find (u_α, κ) such that

$$\Delta u_\alpha(\boldsymbol{x}) = 0 \quad \left(\boldsymbol{x} \in (\Omega_m \cup \Omega_d)\backslash\overline{D_\alpha}\right), \ \Delta_\alpha u_\alpha(\boldsymbol{x}) = 0 \quad \left(\boldsymbol{x} \in (\Omega_m \cup \Omega_d) \cap D_\alpha\right),$$

with the transmission conditions

$$\begin{aligned} u_{\alpha|\Omega_m}(\boldsymbol{x}) &= u_{\alpha|\Omega_d}(\boldsymbol{x}), \ \partial_n u_{\alpha|\Omega_m}(\boldsymbol{x}) = \kappa\, \partial_n u_{\alpha|\Omega_d}(\boldsymbol{x}) && (\boldsymbol{x} \in \partial\Omega_m) \\ u_{\alpha|D_\alpha}(\boldsymbol{x}) &= u_{\alpha|\Omega\backslash\overline{D_\alpha}}(\boldsymbol{x}), \ \alpha\, \partial_n u_{\alpha|D_\alpha}(\boldsymbol{x}) = \partial_n u_{\alpha|\Omega\backslash\overline{D_\alpha}}(\boldsymbol{x}) && (\boldsymbol{x} \in \partial D_\alpha), \end{aligned}$$

and the decay condition at infinity $u_\alpha(\boldsymbol{x}) \underset{|\boldsymbol{x}|\to\infty}{=} O\left(|\boldsymbol{x}|^{-1}\right)$.

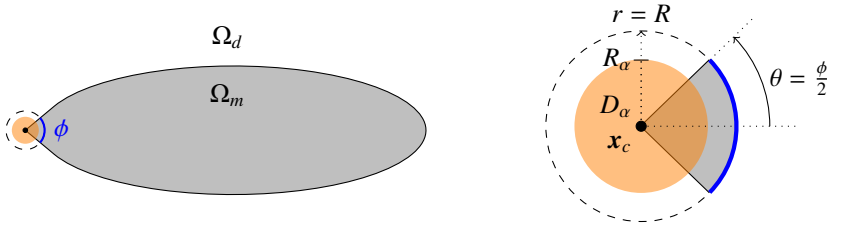

(a) Overview with corner neighborhood highlighted. (b) Corner neighborhoods D and D_α.

Fig. 6: Particle Ω_m with a complex-scaling region $D_\alpha \subset D$ around the corner.

Since the scaling does not affect the orthoradial part of the Laplacian, the PEP and the PEPα share the same corner dispersion relations (7). This implies that Proposition 2 also holds for the PEPα provided that "$r^{i\eta}$" is substituted by "$r^{i\eta/\alpha}$". We introduce the *critical curves*

$$I_c^{\mathfrak{e}(\mathfrak{o}),\alpha} := \left\{\kappa \in \mathbb{C} \,\middle|\, \exists \eta \in H_\phi^{\mathfrak{e}(\mathfrak{o})}(\kappa)\backslash\{0\} : \ \frac{\eta}{\alpha} \in \mathbb{R}\right\}, \ I_c^{\alpha} := I_c^{\mathfrak{e},\alpha} \cup I_c^{\mathfrak{o},\alpha}, \tag{30}$$

which when $\alpha \in \mathbb{R}^*$ coincide with the critical intervals $I_c^{\mathfrak{e}(\mathfrak{o})}$ and I_c respectively. An isolated eigenvalue $\kappa \notin \overline{I_c^{\alpha}}$ of the PEPα is associated with an eigenfunction that admits the local expansion

$$u_\alpha(r,\theta) \underset{r\to 0}{=} c_0 + \sum_{\substack{\eta \in \widehat{H}_\phi^{\mathfrak{e},\alpha}(\kappa) \\ \eta_\star < \Im\left(\frac{\eta}{\alpha}\right)}} c_\eta^{\mathfrak{e}}\, r^{i\frac{\eta}{\alpha}} \Phi_\eta^{\mathfrak{e}}(\theta) + \sum_{\substack{\eta \in \widehat{H}_\phi^{\mathfrak{o},\alpha}(\kappa) \\ \eta_\star < \Im\left(\frac{\eta}{\alpha}\right)}} c_\eta^{\mathfrak{o}}\, r^{i\frac{\eta}{\alpha}} \Phi_\eta^{\mathfrak{o}}(\theta) + O\left(r^{-\eta_\star}\right) \quad (r \in (0, R_\alpha), \ \theta \in (-\pi, \pi]) \tag{31}$$

for any $\eta_\star < 0$, where

$$\widehat{H}_\phi^{\mathfrak{e}(\mathfrak{o}),\alpha}(\kappa) := \left\{\eta \in H_\phi^{\mathfrak{e}(\mathfrak{o})}(\kappa) \,\middle|\, \Im\left(\eta/\alpha\right) < 0\right\}, \ \widehat{H}_\phi^{\alpha}(\kappa) := \widehat{H}_\phi^{\mathfrak{e},\alpha}(\kappa) \cup \widehat{H}_\phi^{\mathfrak{o},\alpha}(\kappa)$$

are the sets of stable zeros that we associate with the PEPα, which reduce to $\widehat{H}_\phi^{\mathfrak{e}(\mathfrak{o})}(\kappa)$ and $\widehat{H}_\phi(\kappa)$ when $\alpha > 0$. The next section explains how the PEPα can be used to compute CP resonances.

3.2. Computation of complex plasmonic resonances

Assume $\kappa \notin \mathbb{R}$ is an isolated eigenvalue of the PEPα. For κ to be an even-critical (resp. odd-critical) CP resonance, the scaling parameter α must be chosen so that

$$\widehat{H}_\phi^{\alpha}(\kappa) = \widehat{H}_\phi^{|\mathfrak{e}(\mathfrak{o})}(\kappa), \tag{32}$$

i.e. the set of zeros that are stable after a rotation of angle $-\arg(\alpha)$ is exactly $\widehat{H}_\phi^{|\mathfrak{e}(\mathfrak{o})}(\kappa)$. The condition (32) can be read as a constraint on α given κ. However in practice α is an input parameter so it is also useful to consider it as a constraint on κ given α: it effectively delimits a region of the complex plane given by

$$K_\phi^{\mathfrak{e}(\mathfrak{o}),\alpha} := \{\kappa \in \mathbb{C} \,|\, \text{Stability condition (32) holds}\},$$

which is where computable CP resonances lie. The link between isolated eigenvalues of the PEPα and CP resonances is given in the next proposition (the odd variant is obtained by replacing "$\mathfrak{e}$" by "$\mathfrak{o}$").

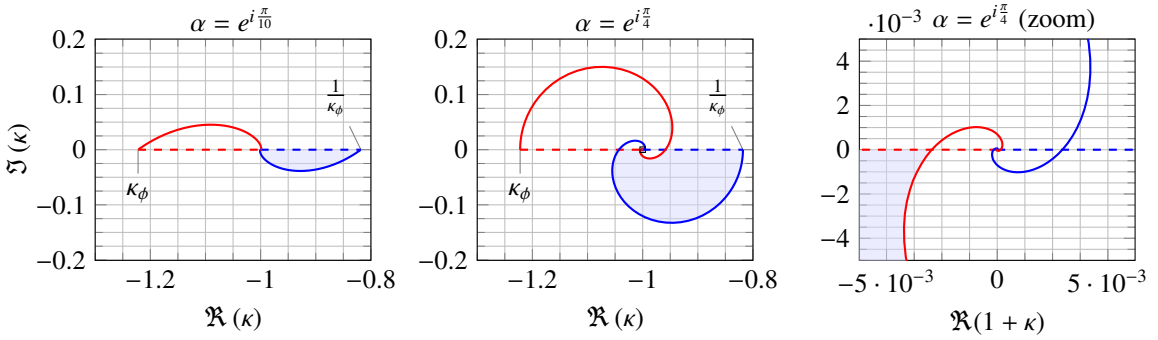

Fig. 7: Even uncovered region $U_\phi^{\mathfrak{e},\alpha}$ for $\phi = 0.9\pi$ and two values of $\arg(\alpha)$ in $[0, \pi/2]$. (—): even critical curve $I_c^{\mathfrak{e},\alpha}$, (—): $I_c^{\mathfrak{o},\alpha}$.

Proposition 17. *Let $\alpha \in \mathbb{C}\backslash\mathbb{R}$. Let (u_α, κ) be a solution of the* PEPα *such that κ belongs to the* even uncovered region

$$U_\phi^{\mathfrak{e},\alpha} := K_\phi^{\mathfrak{e},\alpha} \cap \overline{\mathbb{C}^-}. \tag{33}$$

If $\Im(\kappa) < 0$ (resp. $\Im(\kappa) = 0$) then κ is an even-critical CP resonance (resp. EP eigenvalue) and the function defined by

$$u(\boldsymbol{x}) := u_\alpha(\boldsymbol{x}) \quad \left(\boldsymbol{x} \in (\Omega_m \cup \Omega_d)\backslash\overline{D_\alpha}\right), \; u(r,\theta) := u_\alpha(r^\alpha, \theta) \quad \left(r \in (0, R_\alpha), \; \theta \in (-\pi, \pi]\right)$$

is its associated CP resonance function (resp. eigenfunction).

Proof. Since κ is an isolated eigenvalue of the PEPα, u_α admits the expansion (31) at the corner. The substitution $r \to r^\alpha$ in (31) yields the expansion of u at the corner (this is not a change of variable but an analytic continuation of $u_\alpha(\cdot,\theta)$ from $(0,R_\alpha) \subset \mathbb{R}$ to $(0,R_\alpha)^\alpha \subset \mathbb{C}$, which we do not further justify here). u solves the PEP (1,2,3) and satisfies

$$u(r,\theta) \underset{r\to 0}{=} c_0 + \sum_{\substack{\eta \in \widetilde{H}_\phi^{\mathfrak{e},\alpha}(\kappa) \\ \eta_\star < \Im(\eta)}} c_\eta^{\mathfrak{e}} \, r^{i\eta} \Phi_\eta^{\mathfrak{e}}(\theta) + \sum_{\substack{\eta \in \widetilde{H}_\phi^{\mathfrak{o},\alpha}(\kappa) \\ \eta_\star < \Im(\eta)}} c_\eta^{\mathfrak{o}} \, r^{i\eta} \Phi_\eta^{\mathfrak{o}}(\theta) + O\left(r^{-\eta_\star}\right) \quad (r \in (0,R), \; \theta \in (-\pi,\pi])$$

for any $\eta_\star < 0$ so that, using the stability condition (32), it is an even-critical EP eigenvalue or CP resonance. □

If $\alpha \in \mathbb{R}^*$, $U_\phi^{\mathfrak{e}(\mathfrak{o}),\alpha}$ is empty since $K_\phi^{\mathfrak{e}(\mathfrak{o}),\alpha} = \mathbb{C}^+$. From the above result, the usefulness of the PEPα relies on the ability to choose a non-real α so that the uncovered region includes the part of the complex plane where CP resonances are sought.

Let us now discuss how to compute the uncovered region, which is of practical importance to help choose the scaling parameter α. A straightforward method is to sample the complex plane (in κ) and evaluate (32). However this is costly since it requires the accurate computation of the zeros set $H_\phi(\kappa)$, which can be challenging depending on the value of ϕ. A more accurate alternative is to compute the *boundaries* of the uncovered region, which reduces to computing the critical curves (30). Indeed, we have the identities

$$U_\phi^{\mathfrak{e}(\mathfrak{o}),\alpha} := \left\{\kappa \in \overline{\mathbb{C}^-} \,\middle|\, \widehat{H}_\phi^\alpha(\kappa) = \widehat{H}_\phi^{|\mathfrak{e}(\mathfrak{o})}(\kappa)\right\} = \left\{\kappa \in \overline{\mathbb{C}^-} \,\middle|\, \widehat{H}_\phi^\alpha(\kappa) \supset \widehat{H}_\phi^{|\mathfrak{e}(\mathfrak{o})}(\kappa)\right\} = \left\{\kappa \in \overline{\mathbb{C}^-} \,\middle|\, \forall \eta \in \widehat{H}_\phi^{|\mathfrak{e}(\mathfrak{o})}(\kappa), \; \Im\left(\eta/\alpha\right) < 0\right\},$$

so that the boundary satisfies

$$\partial U_\phi^{\mathfrak{e}(\mathfrak{o}),\alpha} = \left\{\kappa \in \overline{\mathbb{C}^-} \,\middle|\, \exists \eta \in \widehat{H}_\phi^{|\mathfrak{e}(\mathfrak{o})}(\kappa), \; \Im\left(\eta/\alpha\right) = 0\right\} \subset \left\{\kappa \in \overline{\mathbb{C}^-} \,\middle|\, \exists \eta \in H_\phi(\kappa)\backslash\{0\}, \; \Im\left(\eta/\alpha\right) = 0\right\} \subset \overline{I_c^\alpha} \cap \overline{\mathbb{C}^-}.$$

The interest of this inclusion is that plotting the critical curves is straightforward when the scaling parameter is contrast-independent, since they then admit the parametric representations

$$I_c^{\mathfrak{e}(\mathfrak{o}),\alpha} = \left\{\kappa \in \mathbb{C} \,\middle|\, \exists \tilde{\eta} > 0 : \; f_\phi^{\mathfrak{e}(\mathfrak{o})}(\alpha\tilde{\eta}, \kappa) = 0\right\} = \left\{ \frac{\psi_\phi\left(\alpha\tilde{\eta}\right)\,{}^{-}_{(+)}1}{\psi_\phi\left(\alpha\tilde{\eta}\right)\,{}^{+}_{(-)}1} \,\middle|\, \tilde{\eta} \in (0,\infty) \right\},$$

where ψ_ϕ is given by (11). These parametric representations show that both intervals are even with respect to α and only depend upon $\arg(\alpha)$, so that from now on we always assume

$$|\alpha| = 1, \; \arg(\alpha) \in \left[-\frac{\pi}{2}, \frac{\pi}{2}\right].$$

Figure 7 plots the even uncovered region for $\phi = 0.9\pi$ and two scaling parameters. (The cases $\phi \in (0,\pi)$ and $\phi \in (\pi, 2\pi)$ are similar, with even and odd switching roles.) When $\alpha \neq 1$, the two critical curves spiral around the branch point $\kappa = -1$, which reflects its logarithmic nature. The plots also highlight the impact of $\arg(\alpha)$ on the uncovered region. The closer $\arg(\alpha)$ is to $\pi/2$, the further away from -1 the even uncovered region is, due to the odd critical curve $I_c^{o,\alpha}$. This shows that there is a trade-off between the area of the uncovered region and how close it gets to -1. Since plasmonic eigenvalues accumulate at -1, practical computations will typically favor small values of $\arg(\alpha)$.

Remark 18. As already stated in Remark 14, starting from $\kappa_0 \in \mathbb{C}^-$ would conjugate everything. In particular, the uncovered region would be included in $\overline{\mathbb{C}^+}$.

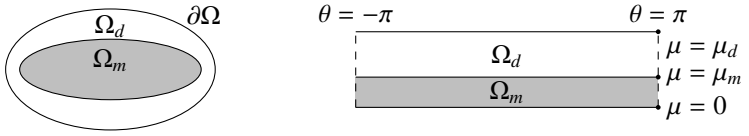

(a) Cartesian coordinates (x, y). (b) Elliptic coordinates (μ, θ) defined by (D.2).

Fig. 8: Elliptical particle in a bounded dielectric domain Ω_d. The boundaries $\partial\Omega_m$ and $\partial\Omega$ are non-circular confocal ellipses.

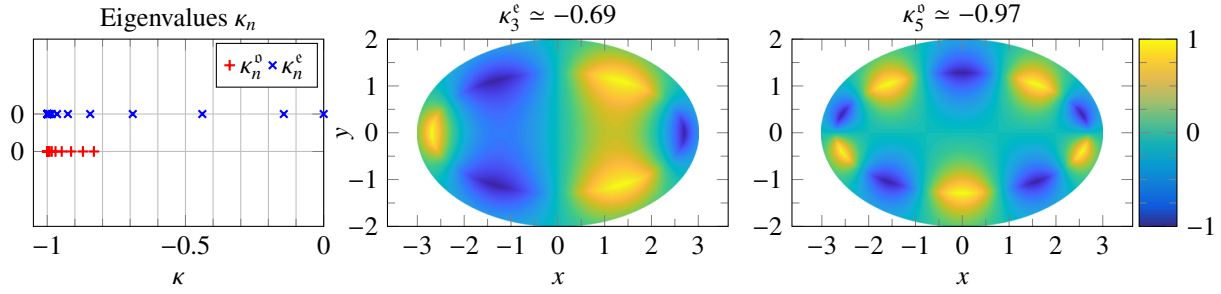

Fig. 9: Eigenvalues (D.1) and eigenfunctions $u/\|u\|_\infty$ of the PEP (35) for an elliptical particle (see Figure 8a). The outer boundary $\partial\Omega$ has semi-axes $a_d = 3$ and $b_d = 2$, and the sign-changing interface $\partial\Omega_m$ is a confocal ellipse such that $a_m = 1.10 \times \sqrt{a_d^2 - b_d^2} \simeq 2.46$.

4. Validation of the finite element discretization

The purpose of this section is to validate the FE discretization of the PEPα that will be used in Section 5 to compute CP resonances. The validation is carried out on two subproblems. Section 4.1 considers an elliptical particle to validate the computation of IP eigenvalues. It highlights that spectral accuracy is strongly controlled by a local mesh symmetry with respect to the sign-changing interface. Section 4.2 considers a corner geometry to validate the discretization of the critical interval, with and without complex scaling.

4.1. Discretization of isolated plasmonic eigenvalues

To validate the discretization of IP eigenvalues, we take

$$\Omega_m := \left\{(x,y) \in \mathbb{R}^2 \,\middle|\, (x/a_m)^2 + (y/b_m)^2 < 1\right\},\ \Omega := \left\{(x,y) \in \mathbb{R}^2 \,\middle|\, (x/a_d)^2 + (y/b_d)^2 < 1\right\},\ \Omega_d := \Omega \backslash \overline{\Omega_m}, \tag{34}$$

with $a_d = 3$, $b_d = 2$, and $a_m = 1.10\sqrt{a_d^2 - b_d^2}$, see Figure 8a. For simplicity we impose a Dirichlet boundary condition on $\partial\Omega$, which excludes the trivial solutions ($u = \text{cst}, \kappa$). The weak formulation of the PEP is then: find $(u, \kappa) \in H_0^1(\Omega) \times \mathbb{C}$ such that for all $v \in H_0^1(\Omega)$,

$$a_{\Omega_m}^{(x,y)}(u,v) = -\kappa\, a_{\Omega_d}^{(x,y)}(u,v), \text{ where } a_X^{(x,y)}(u,v) := \int_X \nabla u(\boldsymbol{x}) \cdot \nabla v(\boldsymbol{x})\, \mathrm{d}\boldsymbol{x}. \tag{35}$$

Since $\partial\Omega_m$ is smooth, the point spectrum is made of a sequence of isolated eigenvalues κ_n that accumulate at $\kappa = -1$ [1, Thm. 1] [33, Thm. A]. Since $\partial\Omega_m$ and $\partial\Omega$ are non-circular confocal ellipses, Laplace's equation (1) is separable in elliptic coordinates and the eigenvalues $\kappa_n^{\mathrm{e(o)}}$ are given by (D.1); the corresponding eigenfunctions are even (resp. odd) with respect to the major axis, see Figure 9. The closer $\kappa_n^{\mathrm{e(o)}}$ is to -1, the more oscillating the eigenfunction.

Remark 19. The distinction between κ_n^{e} and κ_n^{o} is only made in preparation for Section 5.

The PEP (35) can be readily discretized using Lagrange finite elements [54]: after eliminating the DoF on $\partial\Omega$, this leads to the N_h-dimensional generalized eigenvalue problem

$$A_{\Omega_m}^{(x,y)} U = -\kappa A_{\Omega_d}^{(x,y)} U, \tag{36}$$

where A_{Ω_m} and A_{Ω_d} are both real symmetric and positive (but not definite) matrices. In this work, we use the weak form PDE interface of COMSOL 5.4: the FE matrices are obtained using $\mathbb{P}_2$ isoparametric Lagrange elements [55], while the generalized eigenvalue problem is solved using the implicitly restarted Arnoldi method with shift-and-invert from ARPACK [56] with a tolerance of 10^{-6}. To compute a spectrum that spans a large region of $\mathbb{C}$, the eigenproblem is solved several times for various values of the shift κ_0 (which is always taken non-null, since $A_{\Omega_m}^{(x,y)}$ is singular).

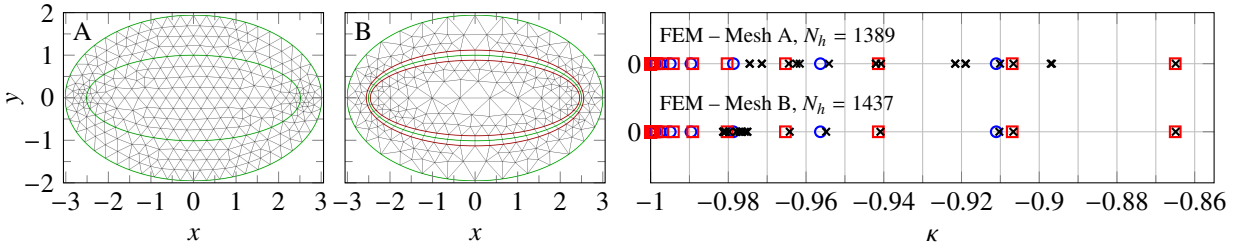

Fig. 10: Solution of the PEP (35). (Left) Mesh A: 616 elements, unstructured. (Center) Mesh B: 574 elements, structured region around $\partial\Omega_m$ built using two ellipses defined though (37) and highlighted in red. (Right) (×): computed, (○): exact even κ_n^{e}, (□): exact odd κ_n^{o}.

Meshing strategy

Let us first consider a triangular mesh symmetric with respect to the x-axis, as depicted in the left graph of Figure 10. The computed spectrum shown in the right plot exhibits significant pollution, with the largest spurious eigenvalue at $\kappa_{\mathrm{sp}} \simeq -0.895$. Figure 11 plots one of the spurious plasmons: in contrast with surface plasmons, which oscillate over the whole interface $\partial\Omega_m$, spurious plasmons are localized at only a few nodes of the interface. This spectral pollution is not caused by a resolution problem, as the mesh used in this example is fine enough to resolve plasmons much closer to -1 than κ_{sp}. In practice, this means that refining the mesh is not an effective strategy to deal with these spurious plasmons, i.e. it does not systematically move the spurious eigenvalues closer to -1. Typically, mesh refinement even spreads spurious eigenvalues and increases κ_{sp}.

An effective strategy to reduce this spectral pollution is to employ a mesh that is structured at the sign-changing interface $\partial\Omega_m$, as depicted in the center graph of Figure 10. The mesh is constructed using two additional confocal

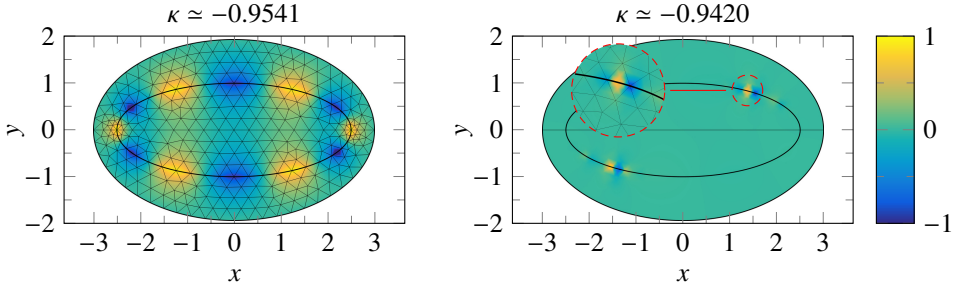

Fig. 11: Eigenfunctions $u/\|u\|_\infty$ computed using the mesh A shown in Figure 10. (Left) Correct eigenfunction (surface plasmon), oscillating over the whole interface. (Right) Spurious eigenfunction (spurious plasmon), localized at only a few nodes of the interface.

ellipses highlighted in red. Crucially, these two ellipses must be chosen so that the structured layer is (approximately) symmetric in elliptic coordinates: first, the semi-axis a_o of the outer ellipse is chosen in (a_m, a_d); then, the inner ellipse is obtained from

$$a_i = c\,\cosh\left[2\mu_m - \mu_o\right] = c\,\cosh\left[2\,\mathrm{acosh}\left(\frac{a_m}{c}\right) - \mathrm{acosh}\left(\frac{a_o}{c}\right)\right], \tag{37}$$

where c is the focal distance of $\partial\Omega_m$. The use of isoparametric elements enables to better approximate the inner and outer ellipses, thus improving the symmetry of the structured layer. In addition, the orthoradial element distribution along $\partial\Omega_m$ is refined in the high-curvature region using an *ad hoc* geometric distribution.

The right plot of Figure 10 shows that spurious eigenvalues have been moved significantly closer to -1, although the number of DoF is similar. This meshing strategy is inspired by the works [57, 58], where the interest of mesh symmetry to discretize sign-changing problems is highlighted and investigated. Based on this result, from now on, all the meshes considered will be structured and (at least approximately) symmetric at the sign-changing interface.

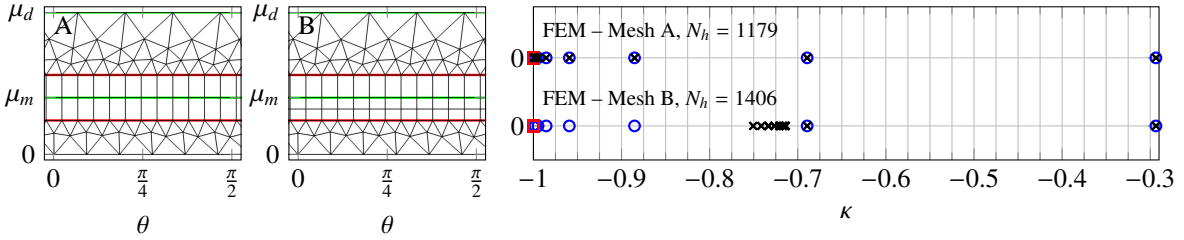

Fig. 12: Solution of the PEP (35) in elliptic coordinates. (Left) Mesh A: 459 elements, symmetric structured layer at the sign-changing interface. (Center) Mesh B: 504 elements, identical to Mesh A except that the symmetry of the structured layer has been broken by sub-dividing one side. (Right) (×): computed, (○): exact even κ_n^{e}, (□): exact odd κ_n^{o}.

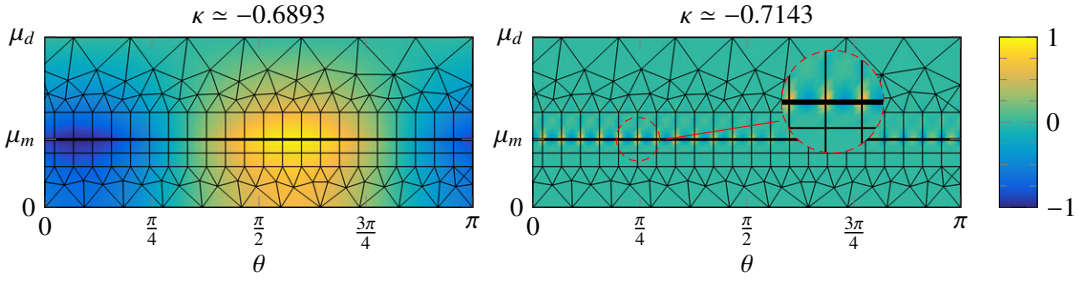

Fig. 13: Eigenfunctions $u/\|u\|_\infty$ using mesh B from Figure 12 ($\mu_m = 0.5$, $\mu_d = 1.25$). (Left) Surface plasmon. (Right) Spurious plasmon.

Justification of the meshing strategy

The meshing strategy proposed above relies on (37) to define the structured layer, which can be justified using the following numerical experiment. Consider the elliptic coordinate system (D.2) associated with $\partial\Omega_m$ (see Figure 8b): the weak formulation is (35) with $\mathrm{d}x = \mathrm{d}\mu\,\mathrm{d}\theta$, $\nabla u = \left[\partial_\mu u, \partial_\theta u\right]$, and periodic boundary conditions. The computed spectra plotted in Figure 12 show that even a small deviation from symmetry with respect to $\{\mu = \mu_m\}$ in the structured layer induces spectral pollution. Figure 13 compares a surface and a spurious plasmon to highlight that the pattern already observed in Cartesian coordinates can be reproduced in elliptic coordinates.

Remark 20. The eigenproblem (36) is sparse and N_h-dimensional. Using static condensation, it can be rewritten as a dense and N_i-dimensional eigenproblem, where N_i is the number of DoF on $\partial\Omega_m$. Based on our numerical experiments (not shown here), static condensation yields no accuracy gain and in particular suffers from the same pollution issue. By contrast, even a crude BE discretization does not suffer from this pollution effect. Intuitively, this confirms that the pollution seen with FE comes from the discretization of the normal direction.

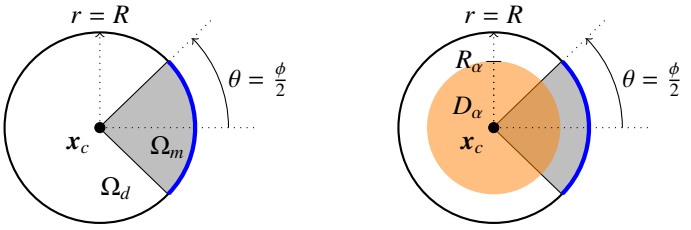

(a) Without complex-scaling region. (b) With complex-scaling region $D_\alpha \subset D$.

Fig. 14: Corner geometry used to validate the discretization of the critical interval.

4.2. *Discretization of the critical interval*

To validate the discretization of I_c and I_c^α we consider the corner geometry (see Figure 14a):

$$\Omega_m := \left\{(x,y) \in \mathbb{R}^2 \;\middle|\; |x+iy| < R,\ |\arg(x+iy)| < \phi/2\right\},\ \Omega := \left\{(x,y) \in \mathbb{R}^2 \;\middle|\; |x+iy| < R\right\},\ \Omega_d := \Omega \backslash \overline{\Omega_m}.$$

Corner without complex scaling

Let us first consider the corner without complex scaling, for which the spectrum of the PEP (35) reduces to the critical interval (10). A natural approach is to mesh in Cartesian coordinates; for a right-angle corner, this can lead to considering a mesh like the one depicted in the left plot of Figure 15, where there is a structured layer around the sign-changing interface. However, the right graph shows that even with a fairly small element size, the critical interval is not satisfactorily resolved.

A first alternative is to mesh in polar coordinates: find $(u,\kappa) \in H^1_p \times \mathbb{C}$ such that for all $v \in H^1_p$,

$$\int_{\Theta_m}\int_{R_{\mathrm{TR}}}^{R} \nabla u \cdot \nabla v \, r \mathrm{d}r\mathrm{d}\theta = -\kappa \int_{\Theta_d}\int_{R_{\mathrm{TR}}}^{R} \nabla u \cdot \nabla v \, r \mathrm{d}r\mathrm{d}\theta, \tag{38}$$

where

$$H^1_p := \left\{u \in H^1\left((R_{\mathrm{TR}},R)\times(-\pi,\pi)\right) \;\middle|\; u(R,\cdot) = 0,\ u(\cdot,+\pi) = u(\cdot,-\pi)\right\},$$

the truncation radius $R_{\mathrm{TR}} \in (0,R)$ enables to avoid a singular integrand (in r), and Θ_m and Θ_d are given by (5). In practice this formulation also suffers from a poor resolution of the critical interval as it prevents from choosing $R_{\mathrm{TR}} \ll R$, which is necessary to capture the asymptotic behavior at $r \to 0$. This issue is fixed by the second and preferred alternative that consists in using the so-called Euler coordinates (z,θ) with $z = \ln r$ [15], for which (38) writes: find $(u,\kappa) \in H^1_e \times \mathbb{C}$ such that for all $v \in H^1_e$,

$$a^{(z,\theta)}_{S_m}(u,v) = -\kappa\, a^{(z,\theta)}_{S_d}(u,v), \text{ where } a^{(z,\theta)}_{X}(u,v) := \int_X \left[\partial_z u\ \partial_\theta u\right] \cdot \left[\partial_z v\ \partial_\theta v\right] \mathrm{d}z\mathrm{d}\theta \tag{39}$$

and

$$S := (\ln R_{\mathrm{TR}}, \ln R)\times(-\pi,\pi),\ S_m := (\ln R_{\mathrm{TR}}, \ln R)\times\Theta_m,\ S_d := S\backslash\overline{S_m},\ H^1_e := \left\{u \in H^1(S) \;\middle|\; \begin{matrix} u(\ln R,\cdot) = 0 \\ u(\cdot,+\pi) = u(\cdot,-\pi)\end{matrix}\right\}.$$

Since I_c is associated with functions that behave as $z \mapsto e^{i\eta_c z}$ towards $z = -\infty$, η_c can be interpreted as a wavenumber. This observation leads to the following two remarks:

- The smaller the truncation radius R_{TR}, the smaller the minimum well-resolved η. In practice, if a well-refined mesh gives a poor resolution of I_c near the endpoints $\kappa_\phi^{\pm 1}$, then R_{TR} should be reduced (this follows from the fact that $\eta_c \to 0$ when $\kappa \to \kappa_\phi^{\pm 1}$).
- The smaller the mesh element size, the larger the maximum well-resolved η_c. In practice, the mesh is chosen coarse enough to avoid an overly dense cluster of eigenvalues at $\kappa = -1$. Indeed, a uniform mesh refinement leads to a non-uniform refinement of I_c, clustered at $\kappa = -1$ (since $|\eta_c| \to \infty$ when $\kappa \to -1$).

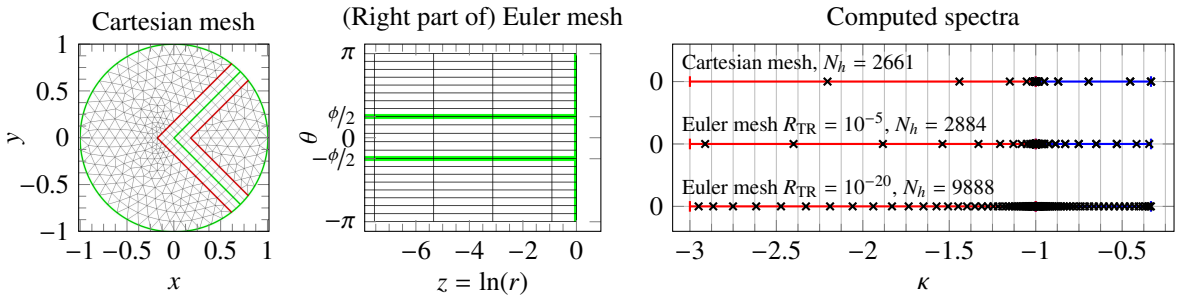

Fig. 15: Comparison between the Cartesian (35) and Euler (39) formulations of the PEP for the corner geometry depicted in Figure 14a with $\phi = \pi/2$ and $R = 1$. (Left) Example of Cartesian mesh. (Center) Example of Euler mesh. (Right) (×): computed, (—): exact even I_c^{e}, (—): exact odd I_c^{o}. The two Euler meshes have the same element size.

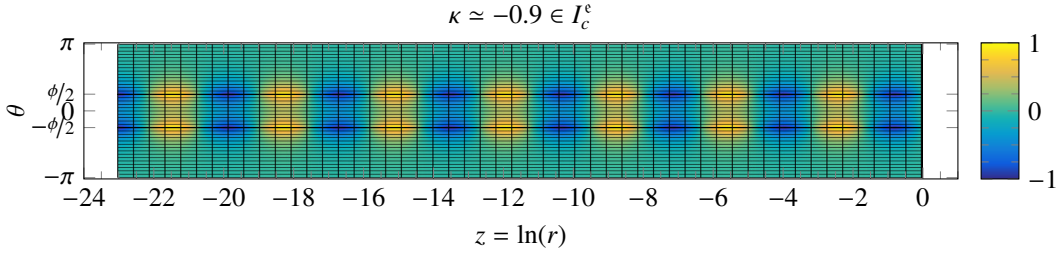

Fig. 16: Eigenfunction $\Re(u)/\|u\|_\infty$ computed using (39) for the corner geometry depicted in Figure 14b with $\phi = \pi/2$, $R = 1$, $R_{\mathrm{TR}} = 10^{-10}$ ($\ln R_{\mathrm{TR}} \simeq -23.02$), and $N_h = 8424$.

The center and right plots of Figure 15 illustrate the mesh and the resolution gain that can be achieved compared to the Cartesian mesh. Figure 16 plots an eigenfunction associated with the discretized critical interval, which highlights one additional advantage of discretizing in Euler coordinates: it will make it easier to identify eigenvalues associated with the critical interval.

Corner with complex scaling

Let us now consider the corner with a complex-scaling region of radius R_α depicted in Figure 14b. Following Section 3.1, the PEPα is naturally formulated in polar coordinates: find $(u, \kappa) \in H^1_p \times \mathbb{C}$ such that for all $v \in H^1_p$,

$$\int_{\Theta_m} \left[\int_{R_\alpha}^{R} \nabla u \cdot \nabla v \, r \mathrm{d}r + \alpha \int_{R_{\mathrm{TR}}}^{R_\alpha} \partial_r u \partial_r v \, r \mathrm{d}r + \frac{1}{\alpha} \int_{R_{\mathrm{TR}}}^{R_\alpha} \partial_\theta u \partial_\theta v \, \frac{\mathrm{d}r}{r} \right] \mathrm{d}\theta = \\ - \kappa \int_{\Theta_d} \left[\int_{R_\alpha}^{R} \nabla u \cdot \nabla v \, r \mathrm{d}r + \alpha \int_{R_{\mathrm{TR}}}^{R_\alpha} \partial_r u \partial_r v \, r \mathrm{d}r + \frac{1}{\alpha} \int_{R_{\mathrm{TR}}}^{R_\alpha} \partial_\theta u \partial_\theta v \, \frac{\mathrm{d}r}{r} \right] \mathrm{d}\theta,$$

which writes in Euler coordinates: find $(u, \kappa) \in H^1_e \times \mathbb{C}$ such that for all $v \in H^1_e$,

$$a^{(z,\theta)}_{S_m \setminus S_\alpha}(u, v) + \alpha \, a^{(z)}_{S_m \cap S_\alpha}(u, v) + \frac{1}{\alpha} a^{(\theta)}_{S_m \cap S_\alpha}(u, v) = -\kappa \left[a^{(z,\theta)}_{S_d \setminus S_\alpha}(u, v) + \alpha \, a^{(z)}_{S_d \cap S_\alpha}(u, v) + \frac{1}{\alpha} a^{(\theta)}_{S_d \cap S_\alpha}(u, v) \right], \tag{40}$$

where $S_\alpha := (\ln R_{\mathrm{TR}}, \ln R_\alpha) \times (-\pi, \pi)$ and

$$a^{(z)}_X(u, v) := \int_X \partial_z u \partial_z v \, \mathrm{d}z\mathrm{d}\theta, \quad a^{(\theta)}_X(u, v) := \int_X \partial_\theta u \partial_\theta v \, \mathrm{d}z\mathrm{d}\theta.$$

Discretizing as in Section 4.1 yields the N_h-dimensional eigenproblem

$$\left[A^{(z,\theta)}_{S_m \setminus S_\alpha} + \alpha \, A^{(z)}_{S_m \cap S_\alpha} + \frac{1}{\alpha} A^{(\theta)}_{S_m \cap S_\alpha} \right] U = -\kappa \left[A^{(z,\theta)}_{S_d \setminus S_\alpha} + \alpha \, A^{(z)}_{S_d \cap S_\alpha} + \frac{1}{\alpha} A^{(\theta)}_{S_d \cap S_\alpha} \right] U, \tag{41}$$

where all the involved matrices are real, symmetric, and positive (but not definite): when $\alpha \notin \mathbb{R}$ the problem is thus complex-symmetric but not Hermitian. This eigenproblem is linear as long as α does not depend upon the contrast.

Figure 17 plots the spectra computed for $\phi = 0.9\pi$ and two scaling parameters. It shows that a satisfactory resolution of the critical curves (30) can be achieved. The corresponding eigenfunctions behave as $e^{i\frac{\eta}{\alpha}z}$ for some $\eta/\alpha \in \mathbb{R}$, so they are similar to the one shown in Figure 16. The next and last section relies on this formulation to compute CP resonances.

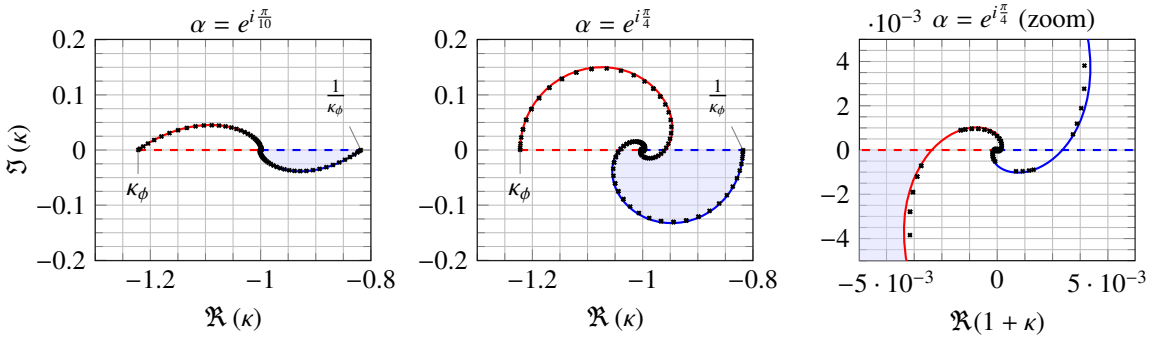

Fig. 17: Comparison between the critical curves (30) and the spectra computed using (41) for the corner geometry depicted in Figure 14b with $\phi = 0.9\pi$, $R = 1$, $R_{\mathrm{TR}} = 10^{-20}$, and $N_h = 9888$. (—): even critical curve $I_c^{\mathrm{e},\alpha}$, (—): $I_c^{\mathrm{o},\alpha}$. (Left) $\alpha = e^{i\frac{\pi}{10}}$. (Center, Right) $\alpha = e^{i\frac{\pi}{4}}$.

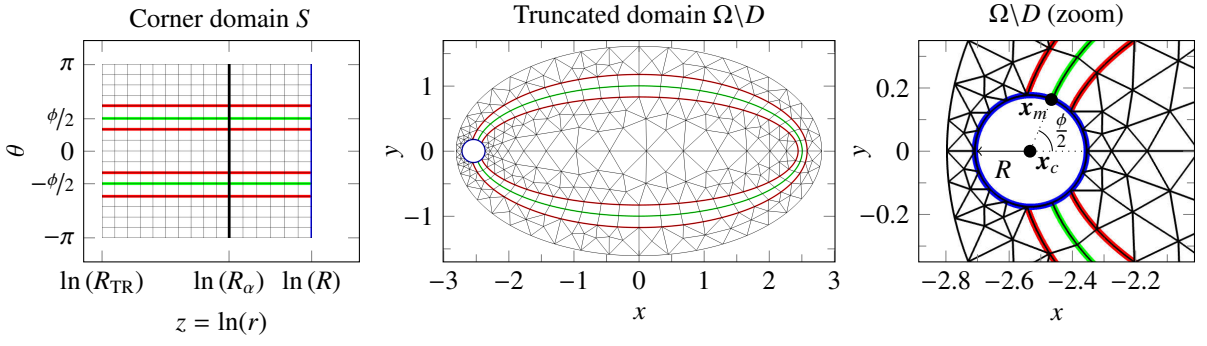

Fig. 18: Mesh topology for a particle Ω_m whose piecewise-smooth boundary $\partial\Omega_m$ (green) is an ellipse perturbed by a corner of angle $\phi \in (0, \pi)$. (Left) Corner domain S, structured mesh. (Center, Right) Domain Ω truncated around $\boldsymbol{x}_c$, mesh with structured layer defined by (37).

5. Complex plasmonic resonances of elliptical particles perturbed by a corner

This section gathers numerical results that illustrate the existence of CP resonances for elliptical particles perturbed by a corner. Section 5.1 describes the particle and its discretization, which mixes Cartesian and Euler coordinates. Section 5.2 discusses the numerical results and shows the agreement with the mechanism described in [35, § 5.2].

5.1. Corner perturbation and weak formulation

We consider an open set Ω_m whose piecewise-smooth boundary is an ellipse of semi-axes (a_m, b_m) perturbed by a corner of angle $\phi \in (0, \pi)$ that is symmetric with respect to the major axis, see Figure 1a. The boundary $\partial\Omega_m$ is uniquely defined by (a_m, b_m, ϕ) since we deduce the remaining geometrical parameters, namely $\boldsymbol{x}_c := (x_c, 0)$ and the top junction point $\boldsymbol{x}_m := (x_m, y_m)$, by imposing a C^1 junction (see the right graph of Figure 18):

$$\left(\frac{x_m}{a_m}\right)^2 + \left(\frac{y_m}{b_m}\right)^2 = 1, \quad x_m = -a_m \frac{\tan\left(\frac{\phi}{2}\right)}{\sqrt{\tan\left(\frac{\phi}{2}\right)^2 + \left(\frac{b_m}{a_m}\right)^2}}, \quad x_c = x_m - \frac{y_m}{\tan\left(\frac{\phi}{2}\right)}.$$

The smaller $\pi - \phi$, the smaller the perturbation radius $R := |\boldsymbol{x}_c - \boldsymbol{x}_m|$. The sets Ω and Ω_d are defined as in (34). Following the results of Section 4, we formulate the discrete problem on the truncated set $\Omega \backslash D_{\mathrm{TR}}$ where $D_{\mathrm{TR}} := \{|\boldsymbol{x} - \boldsymbol{x}_c| < R_{\mathrm{TR}}\}$ with $R_{\mathrm{TR}} \in (0, R]$. The mesh is split into two parts, see Figure 18: the subset $D \backslash D_{\mathrm{TR}}$ is meshed in Euler coordinates while the subset $\Omega \backslash D$ is meshed in Cartesian coordinates with a structured layer at the sign-changing interface $\partial\Omega_m$ defined using (37).

The weak formulation is: find $((u_\alpha, \breve{u}_\alpha), \kappa) \in H^1_{c,e} \times \mathbb{C}$ such that for all $(v, \breve{v}) \in H^1_{c,e}$,

$$\begin{aligned} a^{(x,y)}_{\Omega_m \backslash D}(u_\alpha, v) + a^{(z,\theta)}_{S_m \backslash S_\alpha}(\breve{u}_\alpha, \breve{v}) + \alpha\, a^{(z)}_{S_m \cap S_\alpha}(\breve{u}_\alpha, \breve{v}) + \frac{1}{\alpha}\, a^{(\theta)}_{S_m \cap S_\alpha}(\breve{u}_\alpha, \breve{v}) = \\ - \kappa \left[a^{(x,y)}_{\Omega_d \backslash D}(u_\alpha, v) + a^{(z,\theta)}_{S_d \backslash S_\alpha}(\breve{u}_\alpha, \breve{v}) + \alpha\, a^{(z)}_{S_d \cap S_\alpha}(\breve{u}_\alpha, \breve{v}) + \frac{1}{\alpha}\, a^{(\theta)}_{S_d \cap S_\alpha}(\breve{u}_\alpha, \breve{v}) \right], \end{aligned} \tag{42}$$

with

$$H^1_{c,e} := \left\{ (u, \breve{u}) \in H^1(\Omega \backslash \overline{D}) \times H^1(S) \;\middle|\; \begin{array}{l} u_{|\partial\Omega} = 0,\ \breve{u}(z, +\pi) = \breve{u}(z, -\pi) \quad (z \in (\ln R_{\mathrm{TR}}, \ln R)) \\ u(x_c + R\cos\theta, R\sin\theta) = \breve{u}(\ln R, \theta) \quad (\theta \in (-\pi, \pi]) \end{array} \right\}.$$

This formulation enforces a Neumann boundary condition at the truncation $z = \ln R_{\mathrm{TR}}$. As in Section 4, we employ an isoparametric $\mathbb{P}_2$ Lagrange FE discretization to obtain, after eliminating the DoF on $\partial\Omega$, a N_h-dimensional generalized eigenvalue problem. This eigenvalue problem is linear since α is chosen to be contrast-independent.

Remark 21 (On the choice of a bounded Ω_d). The definitions and results of Sections 2 and 3 carry over to the case where Ω_d is bounded, since they rely on a *local* analysis in a neighborhood of the corner. Using a Dirichlet boundary condition on $\partial\Omega$ will enable us to keep the discussion focused on the corner discretization; using instead a Dirichlet-to-Neumann operator would add a κ-independent term to (42), which if discretized adequately would not change the conclusions (the formula for $\kappa_n^{\mathrm{e(o)}}$ (D.1) still applies to the unbounded case).

5.2. *Numerical results*

Throughout this section the parameters of the unperturbed ellipse are

$$a_m = 2.5,\ b_m = 1,\ c := \sqrt{a_m^2 - b_m^2}.$$

We will consider two geometrical cases (A and B) that differ by both the angle ϕ of the corner perturbation and the semi-axes (a_d, b_d) of the outer ellipse $\partial\Omega$. Note that the semi-major axis a_d limits the perturbation radius R through the constraint $|x_c| + R < a_d$ (see right plot of Figure 18), so that for a given a_d not all corner angles ϕ are achievable.

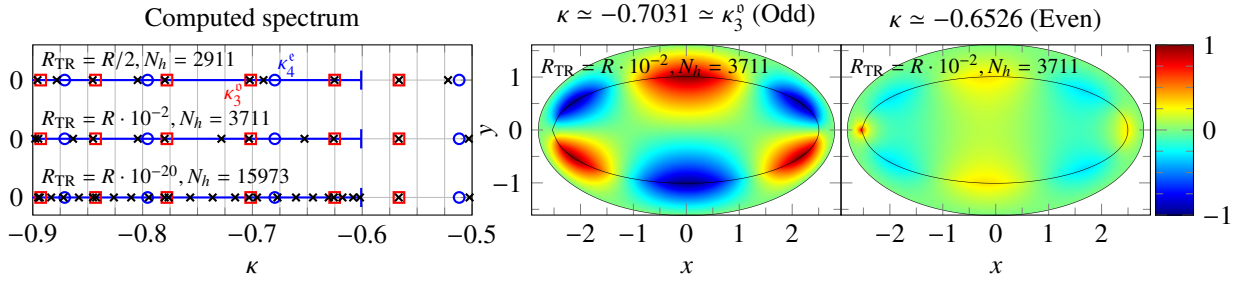

Fig. 19: PEP (42) for the case A parameters (43) and $\alpha = 1$. (Left) (×): computed, (○): κ_n^{e}, (□): κ_n^{o}, (—): I_c^{e}. (Center, Right) Computed eigenfunctions $u/\|u\|_\infty$ associated with a contrast inside I_c^{e}. The corner domain S has been mapped to ease the visualization.

Case A: computation of complex plasmonic resonances

Key to the construction of CP resonances is the local symmetry at the corner, which here (by design) coincides with the symmetry with respect to the major axis. The purpose of this first numerical experiment is to highlight the different behaviors of even and odd eigenfunctions when the corner perturbation is applied. To this end, we choose the geometrical parameters as follows:

$$\phi = 0.75\pi,\ a_d = |x_c| + 1.5R,\ b_d = \sqrt{a_d^2 - c^2}. \tag{43}$$

The corresponding outer ellipse $\partial\Omega$ satisfies $\mu_d \in (\mu_m, 2\mu_m)$ so that all the exact unperturbed eigenvalues κ_n^{e} and κ_n^{o} belong to $(-1, 0]$, see (D.1). As a result, we will focus our interest in the region $\{\Re(\kappa) > -1\}$.

Let us first consider the PEP (42) without complex scaling, i.e. $\alpha = 1$. If $R_{\mathrm{TR}} = R$, the particle Ω_m is an ellipse truncated by a disc of radius R_{TR} centered on $\boldsymbol{x}_c$; if $R_{\mathrm{TR}} < R$, the particle is an ellipse perturbed by a truncated corner. In the limit $R_{\mathrm{TR}} \to 0$ the truncated corner tends to a corner. Figure 19 highlights the different behaviors of odd and even eigenfunctions as R_{TR} is reduced. The left graph shows the eigenvalues computed for various R_{TR}. Overall, odd eigenvalues are significantly less perturbed than their even counterparts. As R_{TR} is reduced, even eigenvalues in I_c^{e} gets significantly perturbed, their density increasing so as to progressively form I_c^{e}. By contrast, even eigenvalues outside I_c remain isolated regardless of the value of R_{TR}.

The center and right graphs of Figure 19 plot two eigenfunctions obtained for a relatively large truncation radius $R_{\mathrm{TR}} = 10^{-2} \cdot R$, which ensures that the corresponding eigenvalues are clearly isolated in the computed spectrum. This illustrates that while odd eigenfunctions undergo very little perturbation when R_{TR} is reduced, even eigenfunctions concentrate at the corner in an increasingly singular fashion.

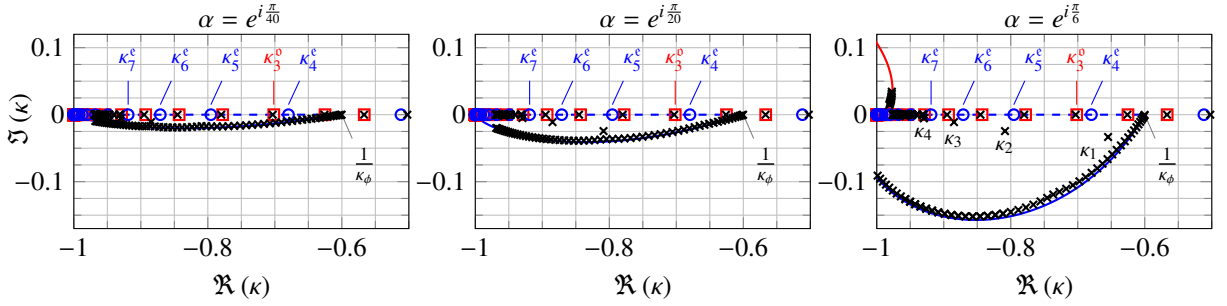

Fig. 20: PEP (42) for the case A parameters (43) and increasing values of $\arg(\alpha)$. (×): computed ($N_h = 26345$, $R_\alpha = R/2$, $R_{\mathrm{TR}} = 10^{-50} \cdot R$), (○): unperturbed even eigenvalues κ_n^{e}, (□): κ_n^{o}, (—): even critical curve $I_c^{\mathrm{e},\alpha}$, (—): $I_c^{\mathrm{o},\alpha}$.

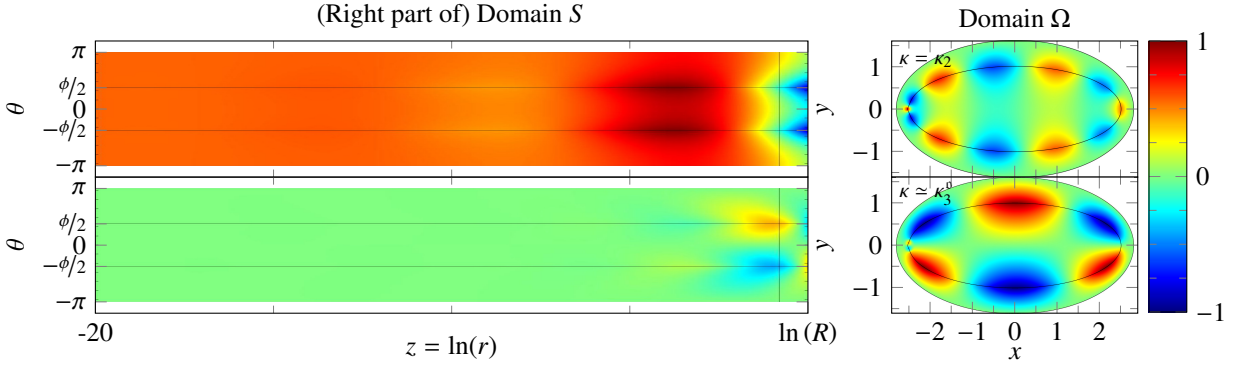

Fig. 21: Eigenfunctions $\Re(u_\alpha)/\|u_\alpha\|_\infty$ of PEP (42) associated with Figure 20 ($\alpha = e^{i\frac{\pi}{6}}$). (Top row) $\kappa = \kappa_2 \simeq 0.8086 - 0.02445i$, even-critical CP resonance. (Bottom row) $\kappa \simeq 0.70313 - 8.0357 \cdot 10^{-8} i \simeq \kappa_3^{\mathrm{o}}$, even-critical EP eigenvalue.

Intuitively, using a suitable $\alpha \neq 1$ will dissipate energy at the corner and tame the singularity. Figure 20 plots the spectra computed for various values of $\arg(\alpha)$. The radius $R_{\mathrm{TR}} = 10^{-50}$ is chosen to ensure a well-resolved critical curve, but such a small value is not necessary to obtain CP resonances in this case. A first observation is that the eigenvalues κ_n^{o} that belong to I_c^{e} have stayed real and have been perturbed into even-critical EP eigenvalues. This can be justified by noting that the corresponding eigenfunctions are odd and therefore their local expansions (27) cannot include the even black-hole wave $u_{\eta_{\mathrm{bh}}^{\mathrm{e}}}$. The bottom row of Figure 21 plots the complex-scaled eigenfunction $\breve{u}_\alpha$ associated with the contrast $\kappa \simeq \kappa_3^{\mathrm{o}}$, which satisfies $\breve{u}_\alpha(z, \theta) \underset{z \to -\infty}{\to} 0$.

By contrast, the eigenvalues κ_n^{e} that belong to I_c^{e} have not stayed real and have been perturbed into even-critical CP resonances: four of them can be seen in Figure 20, which have arisen from κ_4^{e}, κ_5^{e}, κ_6^{e}, and κ_7^{e}. The local expansions (27) of the associated CP resonance functions include a non-null contribution from the even black-hole wave, so

they blow up like (28). The complex-scaled resonance functions behave as $\check{u}_\alpha(z,\theta) \underset{z\to-\infty}{\to} c_0$ since the exponentially growing term is dissipated in the complex-scaling region S_α; this is illustrated in the top row of Figure 21 for $\kappa = \kappa_2$. The behavior of CP resonance functions is as follows: the larger $|\Im(\kappa)|$, the larger $|\Im(\eta)|$, so the stronger the corner singularity; the smaller $|\kappa+1|$, the larger $|\Re(\eta)|$, so the stronger the oscillation as $r \to 0$.

The convergence of the computed CP resonances is plotted in the left graph of Figure 22, where the exact values are approximated as those obtained on a fine mesh and the x-axis is normalized with the value $N_h = 26345$ used in Figures 20 and 21. The closer a CP resonance is to -1, the larger its approximation error. The achieved asymptotic convergence rate can be estimated as $O\left(N_h^{-3/2}\right)$. The center and right plots of Figure 22 illustrate the sensitivity to $\arg(\alpha)$ for $N_h = 26345$. These plots emphasize that each CP resonance can only be computed for $\arg(\alpha) \in (\theta_{\min}, \theta_{\max})$, where $\theta_{\min}$ (resp. $\theta_{\max}$) is the value at which the CP resonance enters (resp. leaves) the uncovered region. For example, $\theta_{\min} \in (\pi/10, \pi/6)$ for κ_1 and $\theta_{\max} \in (\pi/4, \pi/3)$ for κ_2 and κ_3.

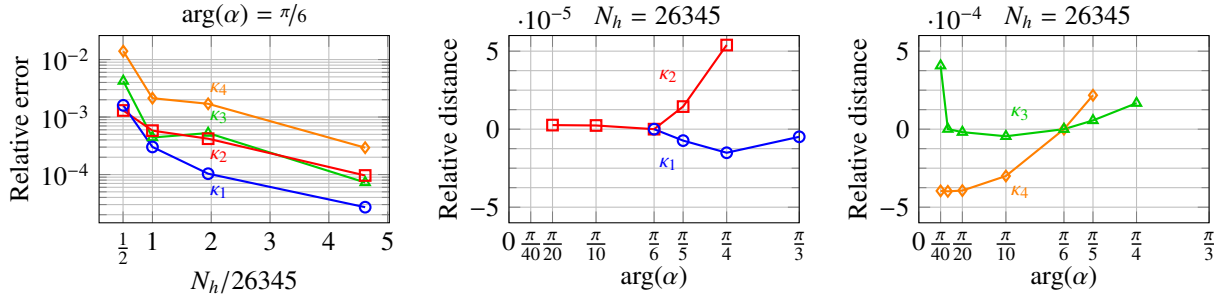

Fig. 22: CP resonances highlighted in Figure 20. (Left) Relative error $|\Im(\kappa_n - \kappa_{n,\text{fine}})|/|\Im(\kappa_{n,\text{fine}})|$ where $\kappa_{n,\text{fine}}$ is the value of κ_n computed with $N_h = 3,976,233$. N_h is varied by changing the mesh in both S and $\Omega\backslash D$, in order to control the maximum element growth rate. (Center and Right) Relative distance $|\Im(\kappa_n - \kappa_{n,\text{ref}})|/|\Im(\kappa_{n,\text{ref}})|$ where $\kappa_{n,\text{ref}}$ is the value of κ_n at $\alpha = e^{i\frac{\pi}{6}}$.

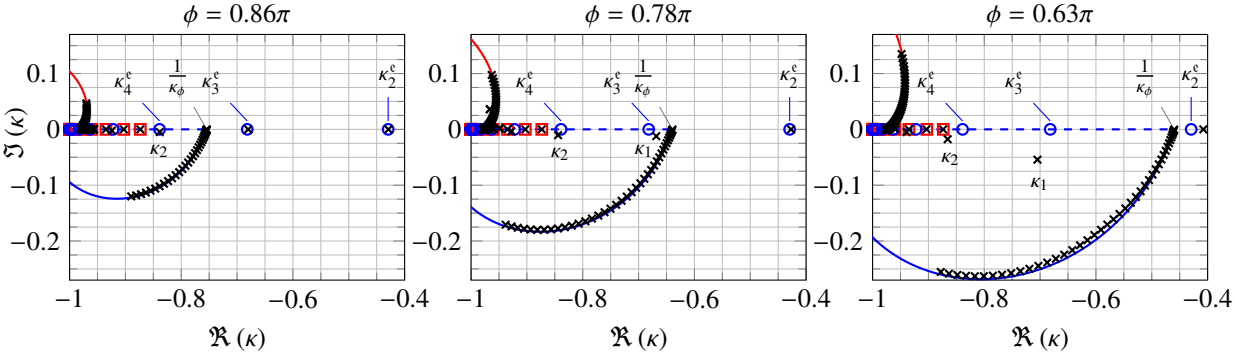

Fig. 23: PEP (42) for the case B parameters (44) and increasing perturbation radius R (i.e. decreasing corner angle ϕ). (×): computed ($N_h = 35695$, $R_\alpha = R/2$, $R_{\text{TR}} = 10^{-50} \cdot R$), (○): unperturbed even eigenvalues κ_n^e, (□): κ_n^o, (—): even critical curve $I_c^{e,\alpha}$, (—): $I_c^{o,\alpha}$.

Case B: dependence on perturbation radius

The purpose of this second numerical experiment is to illustrate the path taken by CP resonances as the perturbation radius R is varied (equivalently: as the corner angle ϕ is varied). Compared to case A we do not change a_m and b_m but we enlarge $\partial\Omega$ so that it can contain the largest corner perturbation considered. Specifically, the chosen geometrical parameters are

$$\frac{\phi}{\pi} \in [0.63, 0.86],\ a_d = [|x_c| + 1.5R]_{|\phi=0.63\pi} \simeq 3.0409,\ b_d = \sqrt{a_d^2 - c^2}. \tag{44}$$

Since a_d is larger than in case A, the exact unperturbed eigenvalues $\kappa_n^{e(o)}$ are different; in particular, the unperturbed eigenvalues κ_n^o are closer to -1. However, we are still in a case where all κ_n^e and κ_n^o belong to $(-1, 0]$.

The results are shown in Figure 23, where $\alpha = e^{i\pi/5}$ has been used. As the perturbation radius is increased, the even critical interval I_c^{e} also increases. Once the eigenvalue κ_3^{e} is reached by I_c^{e}, it gets perturbed into the even-critical CP resonance κ_1, which strays away from the real axis as R is further increased. This behavior differs from that of the eigenvalue κ_2^{e}, which is not reached by I_c^{e} and is thus always perturbed into a real eigenvalue.

The observations made in this section, namely that odd eigenvalues κ_n^{o} in I_c^{e} are perturbed into even-critical EP eigenvalues while even eigenvalues κ_n^{e} in I_c^{e} are perturbed into even-critical CP resonances, are in agreement with the mechanism described in [35, § 5.2].

6. Conclusion and outlook

This paper has investigated the existence of complex plasmonic resonances for a 2D subwavelength particle whose boundary is smooth except for one straight corner.

Section 2 has proposed a definition of complex plasmonic resonances (Definition 13) analogous to that of complex scattering resonances, with the local behavior at the corner playing the role of the behavior at infinity; in particular, complex scattering resonance functions blow up at infinity while complex plasmonic resonance functions blow up at the corner. The construction of the definition has crucially relied on the multivalued nature of the set of stable zeros of the corner dispersion relations (Proposition 9).

Section 3 has shown that isolated eigenvalues of the complex-scaled PEP (Definition 16) that lie inside the so-called uncovered region are embedded plasmonic eigenvalues or complex plasmonic resonances (Proposition 17). The employed complex scaling has been introduced in [15] and can be described as applying a radial scaling in a neighborhood of the corner, see (29). Figure 17 has illustrated how this complex scaling deforms the critical interval, unveiling part of another Riemann sheet where complex plasmonic resonances may be computed.

Thanks to the choice of a κ-independent scaling coefficient α, a standard FE discretization of the complex-scaled PEP has led us to a (complex-symmetric) *linear* generalized eigenvalue problem (42), which is the main computational advantage of this technique over BE methods. However, as has been emphasized in Section 4, the main drawback is the stringent constraint on mesh symmetry at the sign-changing interface.

The numerical results of Section 5 have illustrated the existence of both embedded plasmonic eigenvalues and complex plasmonic resonances for elliptical particles perturbed by a corner. Surface plasmons associated with embedded plasmonic eigenvalues are as regular as surface plasmons associated with isolated plasmonic eigenvalues, while surface plasmons associated with complex plasmonic resonances blow up at the corner like (28). The computed spectra are in agreement with the results presented in [34, Fig. 6], obtained with a rate-of-resonance criterion applied in conjunction with a BE method, which highlighted the presence of embedded plasmonic eigenvalues. In addition, the results also corroborate the mechanism proposed by [35, § 5.2]: even (odd) eigenvalues of the unperturbed ellipse become complex plasmonic resonances if covered by the even (odd) critical interval, while they become embedded plasmonic eigenvalues if covered by the odd (even) critical interval.

Let us mention ideas for future work. Firstly, it would be interesting to drop the quasi-static approximation and compute complex plasmonic resonances using the Helmholtz equation with Drude's model, which yields a nonlinear PEP. Secondly, the computational interest of using a κ-dependent scaling parameter in (42) could be studied, similarly to what has been done in [59] for scattering problems. Thirdly, the 3D extension of the employed complex scaling could be considered: a meaningful starting point would be the rotationally symmetric domains with conical point considered in [60]. Lastly, the design of a BE method to compute complex plasmonic resonances would enable interesting comparison with the FE results presented here.

Acknowledgment

This research has been partly financially supported by the Saclay regional center of INRIA.

A. Corner dispersion relations

This section recalls the derivation of the two corner dispersion relations (7), see also [11, 15]. For any $\eta \in \mathbb{C}$, we define the orthoradial functions

$$\Phi_\eta^{\mathrm{e}}(\theta) := +\frac{\cosh\left[\eta\theta\right]}{\cosh\left[\eta\frac{\phi}{2}\right]}\mathbb{1}_{\Theta_m}(\theta) + \frac{\cosh\left[\eta(\pi-|\theta|)\right]}{\cosh\left[\eta(\pi-\frac{\phi}{2})\right]}\mathbb{1}_{\Theta_d}(\theta), \tag{A.1}$$

$$\Phi_\eta^{\mathfrak{o}}(\theta) \coloneqq +\frac{\sinh\left[\eta\theta\right]}{\sinh\left[\eta\frac{\phi}{2}\right]}\,\mathbb{1}_{\Theta_m}(\theta) + \operatorname{sign}(\theta)\,\frac{\sinh\left[\eta(\pi-|\theta|)\right]}{\sinh\left[\eta\left(\pi-\frac{\phi}{2}\right)\right]}\,\mathbb{1}_{\Theta_d}(\theta), \tag{A.2}$$

where Θ_m and Θ_d are given by (5), and $\mathbb{1}_X$ is the characteristic function of X. Note that $\Phi_0^{\mathfrak{e}}(\theta) = 1$, while $\Phi_0^{\mathfrak{o}}$ is an odd piecewise-linear function.

Proposition 22 (Periodic transmission problem)**.** *Let $\phi \in (0,2\pi)\setminus\{\pi\}$, $\kappa \in \mathbb{C}$, and $\sigma(\theta) \coloneqq \mathbb{1}_{\Theta_m}(\theta) + \kappa\,\mathbb{1}_{\Theta_d}(\theta)$, where Θ_m and Θ_d are given by (5). The 2π-periodic transmission problem*

$$\partial_\theta\left[\sigma(\theta)\,\partial_\theta u(\theta)\right] = \eta^2\sigma(\theta)\,u(\theta) \quad (\theta\in(-\pi,\pi))$$

admits a solution if and only if $f_\phi^{\mathfrak{e}}(\eta,\kappa)\times f_\phi^{\mathfrak{o}}(\eta,\kappa) = 0$.

- *If $\eta\neq 0$ and $f_\phi^{\mathfrak{e}(\mathfrak{o})}(\eta,\kappa) = 0$, then $u(\theta) = C\,\Phi_\eta^{\mathfrak{e}(\mathfrak{o})}(\theta)$.*
- *If $\eta = 0$ then $f_\phi^{\mathfrak{e}}(\eta,\kappa) = f_\phi^{\mathfrak{o}}(\eta,\kappa) = 0$ and we have*

$$u(\theta) = C\,\Phi_0^{\mathfrak{e}}(\theta) \quad \text{if } \kappa\neq\kappa_\phi,\ u(\theta) = C_1\,\Phi_0^{\mathfrak{e}}(\theta) + C_2\,\Phi_0^{\mathfrak{o}}(\theta) \quad \text{if } \kappa=\kappa_\phi.$$

Proof. The strong form of the transmission problem is

$$u''(\theta) = \eta^2\,u(\theta) \quad (\theta\in(-\pi,-\phi/2)\cup(-\phi/2,\phi/2)\cup(\phi/2,\pi)),$$

with boundary conditions

$$\begin{aligned}
&u(\pi) = u(-\pi) && \text{(A)} && u'(\pi) = u'(-\pi) && \text{(B)}\\
&u_{|\Theta_d}(\phi/2) = u_{|\Theta_m}(\phi/2) && \text{(C)} && u_{|\Theta_d}(-\phi/2) = u_{|\Theta_m}(-\phi/2) && \text{(D)}\\
&\kappa\,u'_{|\Theta_d}(\phi/2) = u'_{|\Theta_m}(\phi/2) && \text{(E)} && \kappa\,u'_{|\Theta_d}(-\phi/2) = u'_{|\Theta_m}(-\phi/2). && \text{(F)}
\end{aligned}$$

(Case $\eta = 0$) Since a fundamental system of solutions is $\theta\mapsto(1,\theta)$, we seek u as a piecewise-linear function

$$u(\theta) = \begin{cases} A_1 + B_1\theta & (\theta\in(-\phi/2,\phi/2))\\ A_2 + B_2\,(\theta-\pi) & (\theta\in(\phi/2,\pi))\\ A_3 + B_3\,(\theta+\pi) & (\theta\in(-\pi,-\phi/2)). \end{cases}$$

The periodicity conditions (A,B) give $A_2 = A_3$ and $B_2 = B_3$. The transmission conditions (E,F) give only one additional constraint $B_1 = \kappa B_2$, so that there remain three DoF A_2, B_2, and A_1. The continuity conditions (C,D) give $A_1 = A_2$ and $[\phi/2 - \pi - \kappa\phi/2]\,B_2 = 0$.

(Case $\eta\neq 0$) A fundamental system of solution is $\theta\mapsto(\cosh(\eta\theta),\sinh(\eta\theta))$, so we seek u as

$$u(\theta) = u^{\mathfrak{e}}(\theta) + u^{\mathfrak{o}}(\theta) = \begin{cases} A_1\cosh(\eta\theta) + B_1\sinh(\eta\theta) & (\theta\in(-\phi/2,\phi/2))\\ A_2\cosh(\eta(\theta-\pi)) + B_2\sinh(\eta(\theta-\pi)) & (\theta\in(\phi/2,\pi))\\ A_3\cosh(\eta(\theta+\pi)) + B_3\sinh(\eta(\theta+\pi)) & (\theta\in(-\pi,-\phi/2)). \end{cases}$$

The boundary conditions yield $A_2 = A_3$, $B_2 = B_3$, and the linear system

$$\begin{bmatrix} \cosh\left(\eta\frac{\phi}{2}\right) & -\cosh\left[\eta\left(\pi-\frac{\phi}{2}\right)\right] & 0 & 0\\ \sinh\left(\eta\frac{\phi}{2}\right) & \kappa\sinh\left[\eta\left(\pi-\frac{\phi}{2}\right)\right] & 0 & 0\\ 0 & 0 & \sinh\left(\eta\frac{\phi}{2}\right) & \sinh\left[\eta\left(\pi-\frac{\phi}{2}\right)\right]\\ 0 & 0 & \cosh\left(\eta\frac{\phi}{2}\right) & -\kappa\cosh\left[\eta\left(\pi-\frac{\phi}{2}\right)\right] \end{bmatrix}\begin{bmatrix} A_1\\ A_2\\ B_1\\ B_2 \end{bmatrix} = 0.$$

This gives the even

$$\kappa\cosh\left(\eta\frac{\phi}{2}\right)\sinh\left[\eta\left(\pi-\frac{\phi}{2}\right)\right] + \sinh\left(\eta\frac{\phi}{2}\right)\cosh\left[\eta\left(\pi-\frac{\phi}{2}\right)\right] = 0 \tag{A.3}$$

and odd

$$\kappa\sinh\left(\eta\frac{\phi}{2}\right)\cosh\left[\eta\left(\pi-\frac{\phi}{2}\right)\right] + \cosh\left(\eta\frac{\phi}{2}\right)\sinh\left[\eta\left(\pi-\frac{\phi}{2}\right)\right] = 0 \tag{A.4}$$

dispersion relations. To obtain (7) we use the identity

$$2(a_1b_1 + a_2b_2) = (a_1+a_2)(b_1+b_2) + (a_1-a_2)(b_1-b_2)$$

combined with the formula for $\sinh(a+b)$ [11, § 4.1]. □

B. Zeros of corner dispersion relations

This section gathers the proofs for some of the results claimed in Sections 2.1 and 2.2.1.

B.1. General properties

Lemma 23 (κ-invariant zeros)**.** *Let $\phi \neq \pi$. The set of κ-invariant zeros of $H_\phi^{\mathfrak{e}(\mathfrak{o})}(\kappa)$ is given by $iq\mathbb{Z}$ if $\phi = \frac{p}{q}\pi$ with p and q coprime integers and reduces to $\{0\}$ otherwise.*

Proof. By definition a scalar η is a κ-invariant zero of $H_\phi^{\mathfrak{e}(\mathfrak{o})}(\kappa)$ if it satisfies *both* $\sinh[\eta\pi] = 0$ and $\sinh[\eta(\pi-\phi)] = 0$. Hence, the set of κ-invariant zeros is given by the intersection $i \times \left[\left(\frac{\pi}{\pi-\phi}\mathbb{Z}\right) \cap \mathbb{Z}\right]$. □

Proof of Lemma 3. (a) For any $\kappa \in \mathbb{C}$, the map $\eta \mapsto f_\phi^{\mathfrak{e}(\mathfrak{o})}(\eta, \kappa)$ is entire so its zeros are isolated and have no accumulation point in $\mathbb{C}$ [61, Thm. 10.18]. (b) Follows directly from the expression of $f_\phi^{\mathfrak{e}(\mathfrak{o})}$. (c) If $\eta \in H_\phi^{\mathfrak{e}}(\kappa) \cap H_\phi^{\mathfrak{o}}(\kappa)$, then $[1+\kappa]\sinh[\eta\pi] = 0$ and $[1-\kappa]\sinh[\eta(\pi-\phi)] = 0$. If $\kappa = 1$, then $\eta\pi = ik\pi$ with $k \in \mathbb{Z}$. If $\kappa = -1$, then $\eta(\pi-\phi) = ik\pi$ with $k \in \mathbb{Z}$. If $\kappa \in \mathbb{C}\backslash\{-1,1\}$, then η solves both $\sinh[\eta\pi] = 0$ and $\sinh[\eta(\pi-\phi)] = 0$, so that the intersection $H_\phi^{\mathfrak{e}}(\kappa) \cap H_\phi^{\mathfrak{o}}(\kappa)$ is *exactly* the set of κ-invariant zeros that is described in Lemma 23. □

Proof of Prop. 4 continued. It remains to prove that η_c, which is isolated from Lemma 3(a), crosses the real axis when κ crosses $I_c^{\mathfrak{e}(\mathfrak{o})}$. Let $(\eta_c, \kappa_c) \in (0,\infty) \times I_c^{\mathfrak{e}(\mathfrak{o})}$. Proposition 8, which is a consequence of the implicit function theorem, gives the existence of a neighborhood V of κ_c in $\mathbb{C}\backslash\{\kappa_\phi, 1/\kappa_\phi\}$ such that there is a unique analytic map $\eta : V \to \mathbb{C}$ that satisfies $\eta(\kappa_c) = \eta_c$ and $f(\eta(\kappa), \kappa) = 0$ for all $\kappa \in V$. Since $\eta(\overline{\kappa}) = \overline{\eta(\kappa)}$, $\eta(\kappa)$ must cross the real axis when κ crosses the critical interval $I_c^{\mathfrak{e}(\mathfrak{o})}$ in V. □

Proof of Prop. 8. Let $(\eta_0, \kappa_0) \in \mathbb{C} \times U$ such that $f_\phi^{\mathfrak{e}(\mathfrak{o})}(\eta_0, \kappa_0) = 0$. The claim follows from the implicit function theorem [43, Prop. 2.14]: since $f_\phi^{\mathfrak{e}(\mathfrak{o})}$ is analytic on $\mathbb{C} \times U$, it is enough to show that $\partial_\eta f_\phi^{\mathfrak{e}(\mathfrak{o})}(\eta_0, \kappa_0) \neq 0$. We have

$$\partial_\eta f_\phi^{\mathfrak{e}(\mathfrak{o})}(\eta_0, \kappa_0) = [1+\kappa_0]\,\pi\cosh[\eta_0\pi] \underset{(+)}{-} [1-\kappa_0]\,(\pi-\phi)\cosh[\eta_0(\pi-\phi)].$$

Let us first cover the case $\kappa_0 \in \{-1, 1\}$. If $\kappa_0 = -1$ (resp. $\kappa_0 = 1$) then $\sinh[\eta_0(\pi-\phi)] = 0$ (resp. $\sinh[\eta_0\pi] = 0$) so that $\partial_\eta f_\phi^{\mathfrak{e}(\mathfrak{o})}(\eta_0, \kappa_0) \neq 0$. Now assume that $\kappa_0 \notin \{-1, 1\}$; we show that $\partial_\eta f_\phi^{\mathfrak{e}(\mathfrak{o})}(\eta_0, \kappa_0) = 0 \Leftrightarrow \kappa_0 \in \left\{\kappa_\phi, 1/\kappa_\phi\right\}$. The system $f_\phi^{\mathfrak{e}(\mathfrak{o})}(\eta_0, \kappa_0) = 0$, $\partial_\eta f_\phi^{\mathfrak{e}(\mathfrak{o})}(\eta_0, \kappa_0) = 0$ reads

$$\begin{cases} [1+\kappa_0]\sinh[\eta_0\pi] = \underset{(-)}{+}[1-\kappa_0]\sinh[\eta_0(\pi-\phi)] \\ [1+\kappa_0]\cosh[\eta_0\pi] = \underset{(-)}{+}[1-\kappa_0]\,(1-\phi/\pi)\cosh[\eta_0(\pi-\phi)], \end{cases}$$

which is equivalent to

$$[1+\kappa_0] = \underset{(-)}{+}[1-\kappa_0]\,\psi_\phi(\eta_0),\ \tanh[\eta_0\pi(1-\phi/\pi)] = (1-\phi/\pi)\tanh[\eta_0\pi].$$

Since the only solution of the rightmost equation is $\eta_0 = 0$, the first one is $[1+\kappa_0] = \underset{(-)}{+}[1-\kappa_0]\,\frac{\pi-\phi}{\pi}$. □

Proof of Prop. 9. The proof consists in showing that the set $H_\phi^{\mathfrak{e}(\mathfrak{o})}(\kappa)$ contains a pair of multivalued elements, namely $(\eta_c, -\eta_c)$ where η_c is the critical exponent introduced in Proposition 4. Let us first consider the odd dispersion relation.

(1) Odd dispersion relation. Let $\kappa \in I_c^{\mathfrak{o}}$. The (positive) critical exponent satisfies

$$\frac{1}{\psi_\phi(\eta_c(\kappa))} = \beta(\kappa).$$

The critical exponent is a map $\eta_c : I_c^{\mathfrak{o}} \to (0,\infty)$ and Proposition 8 provides us with an analytic map $\tilde{\eta}_c : V \to \mathbb{C}$ such that $\tilde{\eta}_c(\kappa) = \eta_c$, where V is a neighborhood of κ in $\mathbb{C}\backslash\{\kappa_\phi, 1/\kappa_\phi\}$. (a) The asymptotic expansion

$$\frac{1}{\psi_\phi(\eta)} \underset{\eta\to 0}{=} \frac{\pi}{\pi-\phi}\left[1 + \frac{1}{6}\eta^2\left(\pi^2 - (\pi-\phi)^2\right) + O\left(|\eta|^4\right)\right]$$

yields

$$[\tilde{\eta}_c(\kappa)]^2 \underset{\kappa\to\kappa_\phi}{=} \frac{6(1-\phi/\pi)}{\pi^2\left[1-(1-\phi/\pi)^2\right]}\left(\beta(\kappa)-\beta\left(\kappa_\phi\right)\right)+O\left(|\beta(\kappa)-\beta(\kappa_\phi)|^2\right).$$

By using the exact same reasoning as in Example 7, we deduce that $\kappa \mapsto \widehat{H}^{\mathfrak{o}}_\phi(\kappa)$ has an algebraic branch point at $\kappa=\kappa_\phi$. (b) The asymptotic expansions

$$\frac{1}{\psi_\phi(\eta)} \underset{\Re(\eta)\to+\infty}{\overset{\phi\in(0,\pi)}{=}} e^{\eta\phi}\left[1+O\left(e^{-2\Re(\eta)(\pi-\phi)}\right)\right],\ \frac{1}{\psi_\phi(\eta)} \underset{\Re(\eta)\to+\infty}{\overset{\phi\in(\pi,2\pi)}{=}} -e^{\eta(2\pi-\phi)}\left[1+O\left(e^{-2\Re(\eta)(\phi-\pi)}\right)\right]$$

give

$$\exp\left[\tilde{\eta}_c(\kappa)\phi\right] \underset{\kappa\to-1}{\overset{\phi\in(0,\pi)}{=}} \beta(\kappa)\left[1+O\left(\frac{1}{|\beta(\kappa)|^{2\frac{\pi-\phi}{\phi}}}\right)\right],\ \exp\left[\tilde{\eta}_c(\kappa)(2\pi-\phi)\right] \underset{\kappa\to-1}{\overset{\phi\in(\pi,2\pi)}{=}} -\beta(\kappa)\left[1+O\left(\frac{1}{|\beta(\kappa)|^{2\frac{\phi-\pi}{2\pi-\phi}}}\right)\right],$$

from which we deduce that $\kappa \mapsto \widehat{H}^{\mathfrak{o}}_\phi(\kappa)$ has a logarithmic branch point at $\kappa=-1$ (using again the same reasoning as in Example 7).

(2) Even dispersion relation. Identical to the odd case by replacing "β" by "$-\beta$". The asymptotic expansions imply that $\kappa \mapsto \widehat{H}^{\mathfrak{e}}_\phi(\kappa)$ has an algebraic branch point at $\kappa = 1/\kappa_\phi$ and a logarithmic branch point at $\kappa=-1$. □

B.2. Closed form expression

For any couple of integers (p,q) such that $q \geq 2$ and $p/q \in (0,1)\cup(1,2)$, we define the following polynomial of degree $2(q-1)$:

$$P^{(p,q)}_\beta(x) := \sum_{k=0}^{q-1} x^{2k} + \beta\,\mathrm{sign}(q-p)x^{q-|q-p|}\sum_{k=0}^{|q-p|-1} x^{2k}, \tag{B.1}$$

whose roots are stable by inversion.

Proof of Prop. 6. Since $\kappa \neq -1$, the sets $H^{\mathfrak{e}}_\phi(\kappa)$ and $H^{\mathfrak{o}}_\phi(\kappa)$ are given by

$$H^{\mathfrak{e}(\mathfrak{o})}_\phi(\kappa) = \{\eta\in\mathbb{C}\,|\,\sinh(\eta\pi) = \underset{(+)}{-}\beta(\kappa)\sinh\left[\eta(\pi-\phi)\right]\},$$

where $\beta(\kappa)$ is given by (11). We carry out the proof only for $H^{\mathfrak{e}}_\phi$; the proof for $H^{\mathfrak{o}}_\phi$ is deduced with the substitution $\beta\to-\beta$. Let $x=\exp\left(\frac{\eta\pi}{q}\right)$. The statement $\eta\in H^{\mathfrak{e}}_\phi(\kappa)$ is equivalent to the polynomial equation

$$x^{2q}-1 = -\beta(\kappa)\left[x^{2q-p}-x^p\right].$$

– If $\phi\in(0,\pi)$, then $0<p<q$ and we factor by x^p to get $x^{2q}-1=-\beta(\kappa)x^p\left[x^{2(q-p)}-1\right]$.
– If $\phi\in(\pi,2\pi)$, then $q<p<2q$ and we factor by x^{2q-p} to get $x^{2q}-1=+\beta(\kappa)x^{2q-p}\left[x^{2(p-q)}-1\right]$.
In these two cases the claim is obtained using the identity $x^{2n}-1=(x^2-1)\sum_{k=0}^{n-1}x^{2k}$ on both sides and noting that $x^2=1$ has solutions $\eta\in iq\mathbb{Z}$. From Lemma 23, the set $iq\mathbb{Z}$ is exactly the set of of κ-invariant zeros of $H^{\mathfrak{e}}_\phi(\kappa)$. □

Example 24 ($\phi=\pi/2$)**.** $P^{(1,2)}_\beta(x)=x^2+1+\beta x$ has roots given by $x^\pm_\beta=\frac{-\beta\pm\sqrt{\beta^2-4}}{2}$, hence $\check{H}^{\mathfrak{e}}_\phi(\kappa)=\left\{\eta^+_{\beta(\kappa)},\eta^-_{\beta(\kappa)}\right\}$ and $\check{H}^{\mathfrak{o}}_\phi(\kappa)=\left\{\eta^+_{-\beta(\kappa)},\eta^-_{-\beta(\kappa)}\right\}$ where $\eta^\pm_\beta := \frac{2}{\pi}\ln\left(x^\pm_\beta\right)$, which is consistent with [11, § 4.1]. Since $x^+_\beta x^-_\beta=1$, we have $\eta^-_\beta=-\eta^+_\beta$.

Example 25 ($\phi=\pi/3$)**.** $P^{(1,3)}_\beta(x)=x^4+x^2+1+\beta(x^3+x)$. Since the roots of $P^{(1,3)}_\beta$ are stable by inversion, we seek $(\xi_1,\xi_2)\in\mathbb{C}^*\times\mathbb{C}^*$ such that $P^{(1,3)}_\beta(x)=(x-\xi_1)(x-1/\xi_1)(x-\xi_2)(x-1/\xi_2)$, which is equivalent to

$$\frac{1}{\xi_2}+\xi_2+\frac{1}{\xi_1}+\xi_1=-\beta,\ \left(\frac{1}{\xi_2}+\xi_2\right)\times\left(\frac{1}{\xi_1}+\xi_1\right)=-1.$$

This yields the expression of the four roots of $P^{(1,3)}_\beta$:

$$\left\{x^{\pm,i}_\beta\right\}_{i\in\{+,-\}} = \left\{\frac{1}{2}\left(A_i\pm\sqrt{A_i^2-4}\right)\right\}_{i\in\{+,-\}},\ \text{where } A_\pm := \frac{-\beta\pm\sqrt{\beta^2+4}}{2}, \tag{B.2}$$

so that $\check{H}^{\mathfrak{e}}_\phi(\kappa)=\left\{\eta^{\pm,i}_{\beta(\kappa)}\right\}_{i\in\{+,-\}}$ and $\check{H}^{\mathfrak{o}}_\phi(\kappa)=\left\{\eta^{\pm,i}_{-\beta(\kappa)}\right\}_{i\in\{+,-\}}$, where $\eta^{\pm,i}_\beta := \frac{2}{\pi}\ln\left(x^{\pm,i}_\beta\right)$. Note that since $x^{+,\pm}_\beta x^{-,\pm}_\beta=1$, we have $\eta^{-,\pm}_\beta=-\eta^{+,\pm}_\beta$.

C. Comments on the proposed definition of complex plasmonic resonances

This appendix discusses the proposed definition of CP resonances (Definition 13). Let us first recall that the resolvent of a differential operator $\mathcal{A}$ is an operator-valued analytic function $(\mathbb{C}\backslash\sigma) \ni \lambda \mapsto R(\lambda)$ (typically $\lambda = \omega$ or $\lambda = \omega^2$), which is singular at the spectrum $\sigma \subset \mathbb{C}$. If $\mathcal{A}$ has a non-empty and non-countable continuous spectrum σ_c, then R may be multivalued, i.e. it may admit at least one analytic extension $\tilde{R}$ across σ_c that differs from R, so that σ_c is effectively a branch cut of R. This commonly occurs in scattering problems.

In this paper, the denomination "resonance" is used in the sense encountered in scattering; in particular, "resonance" is not synonymous with "eigenvalue". The operator-theoretic definition of resonances is as follows [36, 37] [62] [63]: for a problem with a multivalued resolvent operator, eigenvalues are poles of the principal branch, while complex resonances are poles of the other branche(s). For example, a single degree-of-freedom oscillator has eigenvalues (complex if damped) but no complex resonances, since the resolvent operator is not multivalued. By contrast, in scattering, the resolvent operator that gives the outgoing solution is multivalued since the spatial domain is unbounded: there can be both eigenvalues and complex resonances. An eigenvalue is associated with a finite-energy eigenfunction, while a complex resonance (also "complex scattering resonance" or "complex scattering pole") is associated with a complex resonance function (also "quasi-normal mode"), whose energy is infinite.

This operator-theoretic approach could be followed to define CP resonances. The "outgoing resolvent operator" R_{out} would be defined using an inverse Mellin transform around the corner [38]. The map $\kappa \mapsto R_{\text{out}}(\kappa)$, naturally defined in $\mathbb{C}^+$ would have branch points κ_ϕ, κ_ϕ^{-1}, and -1. As such, it would admit at least three different meromorphic continuations to $\mathbb{C}^-$: R_0 (continuation across $\mathbb{R}\backslash\overline{I_c}$), R^{e} (continuation across I_c^{e}), and R^{o} (continuation across I_c^{o}). Even-critical CP resonances would then be poles of R^{e} in $\mathbb{C}^-$.

The approach we have followed in this paper is to define CP resonances through their local expansions at $r = 0$, which only requires the knowledge of the corner dispersion relations (7). This approach is commonly followed in the scattering literature, where complex scattering resonance functions are introduced as solutions of the time-harmonic eigenproblem that are exponentially growing at infinity [52] [50] [59]. This approach suggests that to compute complex resonances this exponential growth must be dealt with, which is the purpose of complex scaling.

D. Point spectrum of elliptical particles

Proposition 26. *Let Ω_m, Ω, and Ω_d be given by (34) with $\overline{\Omega_m} \subset \Omega$. If $\partial\Omega_m$ and $\partial\Omega$ are not circles, then the eigenvalues of the PEP (1,2) with a Dirichlet boundary condition on $\partial\Omega$ are given by*

$$\kappa_0^{\text{e}} = 0,\ \kappa_n^{\text{e}} = -\tanh\left[n\mu_m\right]\tanh\left[n(\mu_d - \mu_m)\right],\ \kappa_n^{\text{o}} = -\frac{\tanh\left[n(\mu_d - \mu_m)\right]}{\tanh\left[n\mu_m\right]} \quad (n \in \mathbb{N}^*), \tag{D.1}$$

where $r_m \in (0,1)$ (resp. $r_d \in (0,1)$) is the aspect ratio of $\partial\Omega_m$ (resp. $\partial\Omega$) and $\mu = \operatorname{arctanh} r$. Eigenfunctions associated with κ_n^{e} (resp. κ_n^{o}) are even (resp. odd) with respect to the major axis.

For any $n \in \mathbb{N}$, $\kappa_n^{\text{e}} \in (-1, 0]$ while for any $n \in \mathbb{N}^*$, $\kappa_n^{\text{o}} \in (-1, 0)$ when $\mu_d < 2\mu_m$ and $\kappa_n^{\text{o}} < -1$ when $\mu_d > 2\mu_m$. In the limit $\mu_d \to \infty$ we recover the eigenvalues of the NP operator on $\partial\Omega_m$ [64, Eq. (4.13)].

Proof. Without loss of generality, we assume that Ω_m is such that $a_m > b_m$ so that its focal distance is $c = \sqrt{a_m^2 - b_m^2}$. Let (μ, θ) be the elliptic coordinates associated with the focal points of $\partial\Omega_m$ (see Figure 8b):

$$x = c\cosh\mu\cos\theta,\ y = c\sinh\mu\sin\theta \quad (\mu > 0, \theta \in (-\pi, \pi)). \tag{D.2}$$

Note that $\{\mu = 0, \theta \in (-\pi, \pi)\}$ corresponds to the segment $(-c, +c) \times \{0\}$. In elliptic coordinates, the PEP reads

$$\frac{1}{c^2}\frac{1}{\sinh^2\mu + \sin^2\theta}\left[\partial_\mu^2 u(\mu,\theta) + \partial_\theta^2 u(\mu,\theta)\right] = 0 \quad (\mu \in (0,\mu_m) \cup (\mu_m, \mu_d)),$$

with boundary conditions

$$u(\mu,-\pi) = u(\mu,\pi) \quad (A) \qquad \partial_\theta u(\mu,-\pi) = \partial_\theta u(\mu,\pi) \quad (B)$$
$$u_{|\Omega_d}(\mu_m,\cdot) = u_{|\Omega_m}(\mu_m,\cdot) \quad (C) \qquad \kappa\,\partial_\mu u_{|\Omega_d}(\mu_m,\cdot) = \partial_\mu u_{|\Omega_m}(\mu_m,\cdot) \quad (D)$$

$$u(\mu_d, \cdot) = 0. \qquad \text{(E)}$$

Injecting $u(\mu,\theta) = \varphi(\mu)\Phi(\theta)$ into the PEP leads to

$$\varphi''(\mu) = n^2\varphi(\mu),\ \Phi(\theta) = C_1\ \cos(n\theta) + D_1\ \sin(n\theta) \quad (n \in \mathbb{Z}),$$

where the constraint $n \in \mathbb{Z}$ follows from the periodicity conditions (A,B). If $n = 0$ and $\kappa \neq 0$, then $u = 0$. If $n = 0$ and $\kappa = 0$, then $u(\mu,\theta) \propto \mathbb{1}_{\Omega_m} + \frac{\mu-\mu_d}{\mu_m-\mu_d}\mathbb{1}_{\Omega_d}$. If $n \neq 0$, we seek φ as

$$\varphi(\mu) = \begin{cases} A_2\cosh(n(\mu-\mu_d)) + B_2\sinh(n(\mu-\mu_d)) & (\mu \in (\mu_m,\mu_d)) \\ A_1\cosh(n\mu) + B_1\sinh(n\mu) & (\mu \in (0,\mu_m))\,. \end{cases}$$

(Even modes, $D_1 = 0$) Conditions (C,D,E) and $\varphi'(0) = 0$ yield $A_2 = B_1 = 0$ and

$$\begin{bmatrix} \cosh(n\mu_m) & -\sinh(n(\mu_m-\mu_d)) \\ n\sinh(n\mu_m) & -n\kappa\cosh(n(\mu_m-\mu_d)) \end{bmatrix}\begin{bmatrix} A_1 \\ B_2 \end{bmatrix} = 0,\ \varphi_n^{\mathfrak{e}}(\mu) = B_2\begin{cases} \sinh(n(\mu-\mu_d)) & (\mu \in (\mu_m,\mu_d)) \\ \frac{\sinh(n(\mu_m-\mu_d))}{\cosh(n\mu_m)}\cosh(n\mu) & (\mu \in (0,\mu_m))\,. \end{cases}$$

(Odd modes, $C_1 = 0$) Conditions (C,D,E) and $\varphi(0) = 0$ yield $A_1 = A_2 = 0$ and

$$\begin{bmatrix} \sinh(n\mu_m) & -\sinh(n(\mu_m-\mu_d)) \\ n\cosh(n\mu_m) & -n\kappa\cosh(n(\mu_m-\mu_d)) \end{bmatrix}\begin{bmatrix} B_1 \\ B_2 \end{bmatrix} = 0,\ \varphi_n^{\mathfrak{o}}(\mu) = B_2\begin{cases} \sinh(n(\mu-\mu_d)) & (\mu \in (\mu_m,\mu_d)) \\ \frac{\sinh(n(\mu_m-\mu_d))}{\sinh(n\mu_m)}\sinh(n\mu) & (\mu \in (0,\mu_m))\,. \end{cases}$$

□

References

[1] D. Grieser, The plasmonic eigenvalue problem, Reviews in Mathematical Physics 26 (03) (2014) 1450005. doi:10.1142/S0129055X14500056.

[2] E. D. Palik, Handbook of Optical Constants of Solids, Academic Press, London, 1998.

[3] D. Jackson, Classical electrodynamics, 3rd Edition, John Wiley & Sons, Hoboken, New Jersey, 1999.

[4] S. Maier, Plasmonics fundamentals and applications, Springer, New York, 2007.

[5] P. Markos, C. Soukoulis, Wave propagation from electrons to photonic crystals and left-handed materials, Princeton University Press, Princeton, New Jersey, 2008.

[6] D. Sarid, W. Challener, Modern Introduction to Surface Plasmons, Cambridge University Press, Cambridge, 2010.

[7] A. V. Zayats, I. I. Smolyaninov, A. A. Maradudin, Nano-optics of surface plasmon polaritons, Physics Reports 408 (3) (2005) 131–314. doi:10.1016/j.physrep.2004.11.001.

[8] D. K. Gramotnev, S. I. Bozhevolnyi, Plasmonics beyond the diffraction limit, Nature photonics 4 (2) (2010) 83–91. doi:10.1038/nphoton.2009.282.

[9] J. Pendry, Negative refraction, Contemporary Physics 45 (3) (2004) 191–202. doi:10.1080/00107510410001667434.

[10] S. A. Ramakrishna, Physics of negative refractive index materials, Reports on Progress in Physics 68 (2) (2005) 449–521. doi:10.1088/0034-4885/68/2/R06.

[11] A.-S. Bonnet-Ben Dhia, L. Chesnel, X. Claeys, Radiation condition for a non-smooth interface between a dielectric and a metamaterial, Mathematical Models and Methods in Applied Sciences 23 (09) (2013) 1629–1662. doi:10.1142/S0218202513500188.

[12] A.-S. Bonnet-Ben Dhia, L. Chesnel, P. Ciarlet, T-coercivity for scalar interface problems between dielectrics and metamaterials, ESAIM: Mathematical Modelling and Numerical Analysis 46 (6) (2012) 1363–1387. doi:10.1051/m2an/2012006.

[13] E. Bonnetier, H. Zhang, Characterization of the essential spectrum of the Neumann-Poincaré operator in 2D domains with corner via Weyl sequences, arXiv preprint arXiv:1702.08127 (2017).

[14] C. Hazard, S. Paolantoni, Spectral analysis of polygonal cavities containing a negative-index material, Annales Henri Lebesgue (In press, hal-01626868).

[15] A.-S. Bonnet-Ben Dhia, C. Carvalho, L. Chesnel, P. Ciarlet, On the use of perfectly matched layers at corners for scattering problems with sign-changing coefficients, Journal of Computational Physics 322 (2016) 224–247. doi:10.1016/j.jcp.2016.06.037.

[16] M. I. Stockman, S. V. Faleev, D. J. Bergman, Localization versus delocalization of surface plasmons in nanosystems: Can one state have both characteristics?, Physical Review Letters 87 (2001) 167401. doi:10.1103/PhysRevLett.87.167401.

[17] G. B. Folland, Introduction to Partial Differential Equations, 2nd Edition, Princeton University Press, Princeton, New Jersey, 1995.

[18] D. Colton, R. Kress, Inverse Acoustic and Electromagnetic Scattering Theory, Springer-Verlag, Berlin, 1998.

[19] F. Ouyang, M. Isaacson, Surface plasmon excitation of objects with arbitrary shape and dielectric constant, Philosophical Magazine B 60 (4) (1989) 481–492. doi:10.1080/13642818908205921.

[20] H. Kang, J. Seo, Recent progress in the inverse conductivity problem with single measurement, in: G. Nakamura, J. Seo, M. Yamamoto (Eds.), Inverse problems and related topics, Chapman & Hall/CRC, Boca Raton, 2000, pp. 69–80.

[21] H. Ammari, P. Millien, M. Ruiz, H. Zhang, Mathematical analysis of plasmonic nanoparticles: The scalar case, Archive for Rational Mechanics and Analysis 224 (2) (2017) 597–658. doi:10.1007/s00205-017-1084-5.

[22] I. D. Mayergoyz, D. R. Fredkin, Z. Zhang, Electrostatic (plasmon) resonances in nanoparticles, Physical Review B 72 (2005) 155412. doi:10.1103/PhysRevB.72.155412.

[23] J. Helsing, A. Karlsson, On a Helmholtz transmission problem in planar domains with corners, Journal of Computational Physics 371 (2018) 315–332. doi:10.1016/j.jcp.2018.05.044.

[24] H. Ammari, Y. Chow, K. Liu, J. Zou, Optimal shape design by partial spectral data, SIAM Journal on Scientific Computing 37 (6) (2015) B855–B883. doi:10.1137/130942498.

[25] H. Ammari, Y. Deng, P. Millien, Surface plasmon resonance of nanoparticles and applications in imaging, Archive for Rational Mechanics and Analysis 220 (1) (2016) 109–153. doi:10.1007/s00205-015-0928-0.

[26] K. Ando, H. Kang, H. Liu, Plasmon resonance with finite frequencies: a validation of the quasi-static approximation for diametrically small inclusions, SIAM Journal on Applied Mathematics 76 (2) (2016) 731–749. doi:10.1137/15M1025943.

[27] K. Ando, H. Kang, Analysis of plasmon resonance on smooth domains using spectral properties of the Neumann–Poincaré operator, Journal of Mathematical Analysis and Applications 435 (1) (2016) 162–178. doi:10.1016/j.jmaa.2015.10.033.

[28] H. Kang, M. Lim, S. Yu, Spectral resolution of the Neumann–Poincaré operator on intersecting disks and analysis of plasmon resonance, Archive for Rational Mechanics and Analysis 226 (1) (2017) 83–115. doi:10.1007/s00205-017-1129-9.

[29] K.-M. Perfekt, M. Putinar, Spectral bounds for the Neumann-Poincaré operator on planar domains with corners, Journal d'Analyse Mathématique 124 (1) (2014) 39–57. doi:10.1007/s11854-014-0026-5.

[30] H. Ammari, B. Fitzpatrick, H. Kang, M. Ruiz, S. Yu, H. Zhang, Mathematical and computational methods in photonics and phononics, Vol. 235, American Mathematical Society, Providence, Rhode Island, 2018.

[31] K.-M. Perfekt, M. Putinar, The essential spectrum of the Neumann–Poincaré operator on a domain with corners, Archive for Rational Mechanics and Analysis 223 (2) (2017) 1019–1033. doi:10.1007/s00205-016-1051-6.

[32] Y. Luo, J. B. Pendry, A. Aubry, Surface plasmons and singularities, Nano letters 10 (10) (2010) 4186–4191. doi:10.1021/nl102498s.

[33] K.-M. Perfekt, Plasmonic eigenvalue problem for corners: limiting absorption principle and absolute continuity in the essential spectrum, arXiv preprint arXiv:1911.12294 (2019).

[34] J. Helsing, H. Kang, M. Lim, Classification of spectra of the Neumann–Poincaré operator on planar domains with corners by resonance, Annales de l'Institut Henri Poincare (C) Non Linear Analysis 34 (4) (2017) 991–1011. doi:10.1016/j.anihpc.2016.07.004.

[35] W. Li, S. P. Shipman, Embedded eigenvalues for the Neumann-Poincaré operator, Journal of Integral Equations and Applications 31 (4) (2019) 505–534. doi:10.1216/JIE-2019-31-4-505.

[36] M. Zworski, Resonances in physics and geometry, Notices of the AMS 46 (3) (1999) 319–328.

[37] M. Zworski, Mathematical study of scattering resonances, Bulletin of Mathematical Sciences 7 (1) (2017) 1–85. doi:10.1007/s13373-017-0099-4.

[38] M. Dauge, B. Texier, Problèmes de transmission non coercifs dans des polygones, hal-00562329 (1997).

[39] V. A. Kondrat'ev, O. A. Oleinik, Boundary-value problems for partial differential equations in non-smooth domains, Russian Mathematical Surveys 38 (2) (1983) 1–86. doi:10.1070/rm1983v038n02abeh003470.

[40] S. Nazarov, B. Plamenevsky, Elliptic problems in domains with piecewise smooth boundaries, Walter de Gruyter, Berlin, 1994.

[41] M. Costabel, M. Dauge, Singularities of electromagnetic fields in polyhedral domains, Archive for Rational Mechanics and Analysis 151 (2000) 221–276. doi:10.1007/s002050050197.

[42] V. Kozlov, V. Maz'ya, J. Rossman, Spectral problems asociated with corner singularities of solutions to elliptic equations, American Mathematical Society, Providence, Rhode Island, 2001.

[43] W. Ebeling, Functions of Several Complex Variables and Their Singularities, American Mathematical Society, Providence, Rhode Island, 2007.

[44] J. Aguilar, J. M. Combes, A class of analytic perturbations for one-body Schrödinger hamiltonians, Communications in Mathematical Physics 22 (4) (1971) 269–279. doi:10.1007/BF01877510.

[45] E. Balslev, J. M. Combes, Spectral properties of many-body Schrödinger operators with dilatation-analytic interactions, Communications in Mathematical Physics 22 (4) (1971) 280–294. doi:10.1007/BF01877511.

[46] P. Hislop, I. Sigal, Introduction to Spectral Theory with Applications to Schrödinger Operators, Springer, New York, 1996.

[47] J.-P. Berenger, A perfectly matched layer for the absorption of electromagnetic waves, Journal of Computational Physics 114 (2) (1994) 185–200. doi:10.1006/jcph.1994.1159.

[48] W. C. Chew, W. H. Weedon, A 3D perfectly matched medium from modified Maxwell's equations with stretched coordinates, Microwave and Optical Technology Letters 7 (13) (1994) 599–604. doi:10.1002/mop.4650071304.

[49] C. M. Rappaport, Perfectly matched absorbing boundary conditions based on anisotropic lossy mapping of space, IEEE Microwave and Guided Wave Letters 5 (3) (1995) 90–92. doi:10.1109/75.366463.

[50] S. Kim, J. Pasciak, The computation of resonances in open systems using a perfectly matched layer, Mathematics of Computation 78 (267) (2009) 1375–1398. doi:10.1090/S0025-5718-09-02227-3.

[51] S. Dyatlov, M. Zworski, Mathematical Theory of Scattering Resonances, Version 0.1, 2018.

[52] Y. Duan, W. Koch, C. M. Linton, M. McIver, Complex resonances and trapped modes in ducted domains, Journal of Fluid Mechanics 571 (2007) 119–147. doi:10.1017/S0022112006003259.

[53] S. Hein, W. Koch, L. Nannen, Fano resonances in acoustics, Journal of Fluid Mechanics 664 (2010) 238–264. doi:10.1017/S0022112010003757.

[54] A. Ern, J.-L. Guermond, Theory and Practice of Finite Elements, Springer-Verlag, New York, 2004. doi:978-1-4419-1918-2.

[55] M. Lenoir, Optimal isoparametric finite elements and error estimates for domains involving curved boundaries, SIAM Journal on Numerical Analysis 23 (3) (1986) 562–580. doi:10.1137/0723036.

[56] R. B. Lehoucq, D. C. Sorensen, C. Yang, ARPACK Users' Guide, Society for Industrial and Applied Mathematics, 1998. doi:10.1137/1.9780898719628.

[57] C. Carvalho, L. Chesnel, P. Ciarlet, Eigenvalue problems with sign-changing coefficients, Comptes Rendus Mathematique 355 (6) (2017) 671 – 675. doi:10.1016/j.crma.2017.05.002.

[58] A.-S. Bonnet-Ben Dhia, C. Carvalho, P. Ciarlet, Mesh requirements for the finite element approximation of problems with sign-changing coefficients, Numerische Mathematik 138 (4) (2018) 801–838. doi:10.1007/s00211-017-0923-5.

[59] L. Nannen, M. Wess, Computing scattering resonances using perfectly matched layers with frequency dependent scaling functions, BIT Numerical Mathematics 58 (2) (2018) 373–395. doi:10.1007/s10543-018-0694-0.
[60] J. Helsing, K.-M. Perfekt, The spectra of harmonic layer potential operators on domains with rotationally symmetric conical points, Journal de Mathématiques Pures et Appliquées 118 (2018) 235–287. doi:10.1016/j.matpur.2017.10.012.
[61] W. Rudin, Real and Complex Analysis, 3rd Edition, McGraw-Hill Book Company, New York, 1986.
[62] M. Lenoir, M. Vullierme-Ledard, C. Hazard, Variational formulations for the determination of resonant states in scattering problems, SIAM Journal on Mathematical Analysis 23 (3) (1992) 579–608. doi:10.1137/0523030.
[63] A. Aslanyan, L. Parnovski, D. Vassiliev, Complex resonances in acoustic waveguides, The Quarterly Journal of Mechanics and Applied Mathematics 53 (3) (2000) 429–447. doi:10.1093/qjmam/53.3.429.
[64] J. F. Ahner, Some spectral properties of an integral operator in potential theory, Proceedings of the Edinburgh Mathematical Society 29 (3) (1986) 405–411. doi:10.1017/S0013091500017843.